Beamforming Tradeoffs for Initial UE Discovery in Millimeter-Wave MIMO Systems

Vasanthan Raghavan, *Senior Member, IEEE*, Juergen Cezanne, Sundar Subramanian, Ashwin Sampath, and Ozge Koymen

Abstract—Millimeter-wave (mmW) multi-input multi-output (MIMO) systems have gained increasing traction toward the goal of meeting the high data-rate requirements in next-generation wireless systems. The focus of this work is on low-complexity beamforming approaches for initial user equipment (UE) discovery in such systems. Toward this goal, we first note the structure of the optimal beamformer with per-antenna gain and phase control and establish the structure of good beamformers with per-antenna phase-only control. Learning these right singular vector (RSV)-type beamforming structures in mmW systems is fraught with considerable complexities such as the need for a non-broadcast system design, the sensitivity of the beamformer approximants to small path length changes, inefficiencies due to power amplifier backoff, etc. To overcome these issues, we establish a physical interpretation between the RSV-type beamformer structures and the angles of departure/arrival (AoD/AoA) of the dominant path(s) capturing the scattering environment. This physical interpretation provides a theoretical underpinning to the emerging interest on directional beamforming approaches that are less sensitive to small path length changes. While classical approaches for direction learning such as MUltiple SIgnal Classification (MUSIC) have been well-understood, they suffer from many practical difficulties in a mmW context such as a non-broadcast system design and high computational complexity. A simpler broadcast-based solution for mmW systems is the adaptation of limited feedback-type directional codebooks for beamforming at the two ends. We establish fundamental limits for the best beam broadening codebooks and propose a construction motivated by a virtual subarray architecture that is within a couple of dB of the best tradeoff curve at all useful beam broadening factors. We finally provide the received SNR loss-UE discovery latency tradeoff with the proposed beam broadening constructions. Our results show that users with a reasonable link margin can be quickly discovered by the proposed design with a smooth roll-off in performance as the link margin deteriorates. While these designs are poorer in performance than the RSV learning approaches or MUSIC for cell-edge users, their low-complexity that leads to a broadcast system design makes them a useful candidate for practical mmW systems.

Index Terms—Millimeter-wave systems, MIMO, initial UE discovery, beamforming, beam broadening, MUSIC, right singular vector, noisy power iteration, sparse channels.

I. INTRODUCTION

THE ubiquitous nature of communications made possible by the smart-phone and social media revolutions has meant that the data-rate requirements will continue to grow at an exponential pace. On the other hand, even under the most optimistic assumptions, system resources can continue to scale at best at a linear rate, leading to enormous mismatches between supply and demand. Given this backdrop, many candidate solutions have been proposed [1]–[3] to mesh into the patchwork that addresses the 1000-X data challenge [4] — an intermediate stepping stone towards bridging this burgeoning gap.

One such solution that has gained increasing traction over the last few years is communications over the millimeter-wave (mmW) regime [5]–[10] where the carrier frequency is in the 30 to 300 GHz range. Spectrum crunch, which is the major bottleneck at lower/cellular carrier frequencies, is less problematic at higher carrier frequencies due to the availability of large (either unlicensed or lightly licensed) bandwidths. However, the high frequency-dependent propagation and shadowing losses (that can offset the link margin substantially) complicate the exploitation of these large bandwidths. It is visualized that these losses can be mitigated by limiting coverage to small areas and leveraging the small wavelengths that allows the deployment of a large number of antennas in a fixed array aperture.

Despite the possibility of multi-input multi-output (MIMO) communications, mmW signaling differs significantly from traditional MIMO architectures at cellular frequencies. Current implementations[1] at cellular frequencies are on the order of 4×8 with a precoder rank (number of layers) of 1 to 4; see, e.g., [11]. Higher rank signaling requires multiple radio-frequency (RF) chains[2] which are easier to realize at lower carrier frequencies than at the mmW regime. Thus, there has been a growing interest in understanding the capabilities of low-complexity approaches such as beamforming (that require only a single RF chain) in mmW systems [6], [12]–[17]. On the other hand, smaller form factors at mmW frequencies ensure[3] that configurations such as 4×64 (or even higher dimensionalities) are realistic. Such high antenna dimensionalities as well as the considerably large bandwidths at mmW frequencies result

---

[1] In a downlink setting, the first dimension corresponds to the number of antennas at the user equipment end and the second at the base-station end.

[2] An RF chain includes (but is not limited to) analog-to-digital and digital-to-analog converters, power and low-noise amplifiers, upconverters/mixers, etc.

[3] For example, an $N_t = 64$ element uniform linear array (ULA) at 30 GHz requires an aperture of ~ 1 foot at the critical $\lambda/2$ spacing — a constraint that can be realized at the base-station end.

in a higher resolvability of the multipath and thus, the MIMO channel is naturally *sparser* in the mmW regime than at cellular frequencies [10], [14], [18]–[21].

While the optimal right singular vector (RSV) beamforming structure has been known in the MIMO literature [22], an explicit characterization of the connection of this structure to the underlying physical scattering environment has not been well-understood. We start with such an explicit physical interpretation by showing that the optimal beamformer structure corresponds to beam steering across the different paths with appropriate power allocation and phase compensation confirming many recent observations [14], [23]. Despite using only a single RF chain, the optimal beamformer requires per-antenna phase and gain control (in general), which could render this scheme disadvantageous from a cost perspective. Thus, we also characterize the structure and performance of good beamformer structures with per-antenna phase-only control [15], [23]–[25].

Either of these structures can be realized in practice via an (iterative) RSV learning scheme. To the best of our understanding, specific instantiations of RSV learning such as power iteration have not been studied in the literature (even numerically), except in the noise-less case [26]. A low-complexity proxy to the RSV-type beamformer structures is directional beamforming along the dominant path at the millimeter-wave base-station (MWB) and the user equipment (UE). The directional beamforming structure is particularly relevant in mmW systems due to the sparse nature of the channel, and this structure is not expected to be optimal at non-sparse cellular narrowband frequencies. Our studies show that directional beamforming suffers only a minimal loss in performance relative to the optimal structures, rendering the importance of direction learning for practical mmW MIMO systems, again confirming many recent observations [8], [13]–[17], [23], [27].

Such schemes can be realized in practice via direction learning techniques. Direction learning methods such as MUltiple SIgnal Classification (MUSIC), Estimation of Signal Parameters via Rotational Invariance Techniques (ESPRIT) and related approaches [28]–[30] have been well-understood in the signal processing literature, albeit primarily in the context of military/radar applications. Their utility in these applications is as a "super-resolution" method to discern multiple obstacles/ targets given that the pre-beamforming SNR is moderate-to-high, at the expense of array aperture (a large number of antennas) and computations/energy. While MUSIC has been suggested as a possible candidate beamforming strategy for mmW applications, it is of interest to fairly compare different beamforming strategies given a specific objective (such as initial UE discovery).

The novelty of this work is on such a fair comparison between different strategies in terms of: i) architecture of system design (broadcast/unicast solution), ii) resilience/robustness to low pre-beamforming SNR's expected in mmW systems, iii) performance loss relative to the optimal beamforming scheme, iv) adaptability to operating on different points of the tradeoff curve of initial UE discovery latency vs. accrued beamforming gain, v) scalability to beam refinement as a part of the data transfer process, etc. Our broad conclusions are as follows. The fundamental difficulty with any RSV learning scheme is its extreme sensitivity to small path length changes

that could result in a full-cycle phase change across paths, which becomes increasingly likely at mmW carrier frequencies. Further, these methods suffer from implementation difficulties as seen from a system-level standpoint such as a non-broadcast design, poor performance at low link margins, power amplifier (PA) backoff, poor adaptability to different beamforming architectures, etc. In commonality with noisy power iteration, MUSIC, ESPRIT and related approaches also suffer from a non-broadcast solution, poor performance at low link margins and computational complexity.

To overcome these difficulties, inspired by the limited feedback literature [31]–[33], we study the received SNR performance with the use of a globally known directional beamforming codebook at the MWB and UE ends. The simplest codebook of beamformers made of constant phase offset (CPO) array steering vectors (see Fig. 5 for illustration) requires an increasing number of codebook elements as the number of antennas increases to cover a certain coverage area, thereby corresponding to a proportional increase in the UE discovery latency. We study the beam broadening problem of trading off UE discovery latency at the cost of the peak gain in a beam's coverage area [15], [34]. We establish fundamental performance limits for this problem, as well as realizable constructions that are within a couple of dB of this limit at all beam broadening factors (and considerably lower at most beam broadening factors). With beams so constructed, we show that directional beamforming can tradeoff the UE discovery latency substantially for a good fraction of the users with a slow roll-off in performance as the link margin deteriorates. While the codebook-based approach is sub-optimal relative to noisy power iteration or MUSIC, its simplicity of system design and adaptability to different beamforming architectures and scalability to beam refinement makes it a viable candidate for initial UE discovery in practical mmW beamforming implementations. Our work provides further impetus to the initial UE discovery problem (See Sec. V-E for a discussion) that has attracted attention from many related recent works [35]–[37].

Notations: Lower- ($\mathbf{x}$) and upper-case block ($\mathbf{X}$) letters denote vectors and matrices with $\mathbf{x}(i)$ and $\mathbf{X}(i,j)$ denoting the i-th and (i,j)-th entries of $\mathbf{x}$ and $\mathbf{X}$, respectively. $\|\mathbf{x}\|_2$ and $\|\mathbf{x}\|_\infty$ denote the 2-norm and ∞-norm of a vector $\mathbf{x}$, whereas $\mathbf{x}^H$, $\mathbf{x}^T$ and $\mathbf{x}^\star$ denote the complex conjugate Hermitian transpose, regular transpose and complex conjugation operations of $\mathbf{x}$, respectively. We use $\mathbb{C}$ to denote the field of complex numbers, $\mathbb{E}$ to denote the expectation operation and $\chi(\mathcal{A})$ to denote the indicator function of a set $\mathcal{A}$.

II. SYSTEM SETUP

We consider the downlink setting where the MWB is equipped with N_t transmit antennas and the UE is equipped with N_r receive antennas. Let $\mathbf{H}$ denote the $N_r \times N_t$ channel matrix capturing the scattering between the MWB and the UE. We are interested in beamforming (rank-1 signaling) over $\mathbf{H}$ with the unit-norm $N_t \times 1$ beamforming vector $\mathbf{f}$. The system model in this setting is given as

$$\mathbf{y} = \sqrt{\rho_{\mathrm{f}}} \cdot \mathbf{H}\mathbf{f}s + \mathbf{n} \qquad (1)$$

where ρ_f is the pre-beamforming[4] SNR, s is the symbol chosen from an appropriate constellation for signaling with $\mathbf{E}[s] = 0$ and $\mathbf{E}[|s^2|] = 1$, and $\mathbf{n}$ is the $N_r \times 1$ proper complex white Gaussian noise vector (that is, $\mathbf{n} \sim \mathcal{CN}(\mathbf{0}, \mathbf{I})$) added at the UE. The symbol s is decoded by beamforming at the receiver along the $N_r \times 1$ unit-norm vector $\mathbf{g}$ to obtain

$$\widehat{s} = \mathbf{g}^H \mathbf{y} = \sqrt{\rho_f} \cdot \mathbf{g}^H \mathbf{H} \mathbf{f} s + \mathbf{g}^H \mathbf{n}. \tag{2}$$

For the channel, we assume an extended Saleh-Valenzuela geometric model [38] in the ideal setting where $\mathbf{H}$ is determined by scattering over L clusters/paths with no near-field impairments at the UE end and is denoted as follows:

$$\mathbf{H} = \sqrt{\frac{N_r N_t}{L}} \cdot \sum_{\ell=1}^{L} \alpha_\ell \cdot \mathbf{u}_\ell \mathbf{v}_\ell^H. \tag{3}$$

In (3), $\alpha_\ell \sim \mathcal{CN}(0, 1)$ denotes the complex gain[5], $\mathbf{u}_\ell$ denotes the $N_r \times 1$ receive array steering vector, and $\mathbf{v}_\ell$ denotes the $N_t \times 1$ transmit array steering vector, all corresponding to the ℓ-th path. With this assumption, the normalization constant $\sqrt{\frac{N_r N_t}{L}}$ in $\mathbf{H}$ ensures that the standard channel power normalization[6] in MIMO system studies holds. As a typical example of the case where a uniform linear array (ULA) of antennas are deployed at both ends of the link (and without loss of generality pointing along the X-axis in a certain global reference frame), the array steering vectors $\mathbf{u}_\ell$ and $\mathbf{v}_\ell$ corresponding to angle of arrival (AoA) $\phi_{R,\ell}$ and angle of departure (AoD) $\phi_{T,\ell}$ in the azimuth in that reference frame (assuming an elevation angle $\theta_{R,\ell} = \theta_{T,\ell} = 90^\circ$) are given as

$$\mathbf{u}_\ell = \frac{1}{\sqrt{N_r}} \cdot \left[1, e^{jkd_R \cos(\phi_{R,\ell})}, \cdots, e^{j(N_r-1)kd_R \cos(\phi_{R,\ell})} \right]^T \tag{4}$$

$$\mathbf{v}_\ell = \frac{1}{\sqrt{N_t}} \cdot \left[1, e^{jkd_T \cos(\phi_{T,\ell})}, \cdots, e^{j(N_t-1)kd_T \cos(\phi_{T,\ell})} \right]^T \tag{5}$$

where $k = \frac{2\pi}{\lambda}$ is the wave number with λ the wavelength of propagation, and d_R and d_T are the inter-antenna element spacing[7] at the receive and transmit sides, respectively. To simplify the notations and to capture the *constant phase offset* (CPO)-nature of the array-steering vectors and the correspondence with their respective physical angles, we will henceforth denote $\mathbf{u}_\ell$ and $\mathbf{v}_\ell$ above as $\mathrm{CPO}(\phi_{R,\ell})$ and $\mathrm{CPO}(\phi_{T,\ell})$, respectively.

---

[4]The pre-beamforming SNR is the received SNR seen with antenna selection at both ends of the link and under the wide-sense stationary uncorrelated scattering (WSSUS) assumption. This SNR is the same independent of which antenna is selected at either end.

[5]We assume a complex Gaussian model for α_ℓ only for the sake of illustration of the main results. However, all the results straightforwardly carry over to more general models.

[6]The standard normalization that has been used in MIMO system studies is $\mathbf{E}\left[\mathrm{Tr}(\mathbf{H}\mathbf{H}^H)\right] = N_r N_t$. However, as $\{N_r, N_t\}$ increases as is the case with massive MIMO systems such as those in mmW signaling, this normalization violates physical laws and needs to be modified appropriately; see [21], [39] and references therein. Such a modification will not alter the results herein since the main focus is on a performance comparison between different schemes. Thus, we will not concern ourselves with these technical details here.

[7]With the typical $d_R = d_T = \frac{\lambda}{2}$ spacing, we have $kd_R = kd_T = \pi$.

III. OPTIMAL BEAMFORMING AND RSV LEARNING

In terms of performance metric, we are interested in the received SNR in the instantaneous channel setting (that is, $\mathbf{H} = H$), denoted as SNR_{rx} and defined as,

$$\mathrm{SNR}_{rx} \triangleq \rho_f \cdot \frac{|\mathbf{g}^H \mathbf{H} \mathbf{f}|^2 \cdot \mathbf{E}[|s|^2]}{\mathbf{E}\left[|\mathbf{g}^H \mathbf{n}|^2\right]} = \rho_f \cdot \frac{|\mathbf{g}^H \mathbf{H} \mathbf{f}|^2}{\mathbf{g}^H \mathbf{g}} \tag{6}$$

since the achievable rate as well as the error probability in estimating s are captured by this quantity [31], [40], [41]. We are interested in studying the performance loss between the optimal beamforming scheme based on the RSV of the channel and a low-complexity directional beamforming scheme. Towards this goal, we start by studying the structure of the optimal beamforming scheme under various RF hardware constraints. For the link margin, we are interested[8] in low pre-beamforming SNRs.

A. Optimal Beamforming With Full Amplitude and Phase Control

We start with the setting where there is full amplitude and phase control of the beamforming vector coefficients at both the MWB and the UE. Let $\mathcal{F}_2^{N_t}$ denote the class of energy-constrained beamforming vectors reflecting this assumption. That is, $\mathcal{F}_2^{N_t} \triangleq \left\{ \mathbf{f} \in \mathbb{C}^{N_t} : \|\mathbf{f}\|_2 \leq 1 \right\}$. Under perfect channel state information (CSI) of H at both the MWB and the UE, optimal beamforming vectors $\mathbf{f}_{opt}$ and $\mathbf{g}_{opt}$ are to be designed from $\mathcal{F}_2^{N_t}$ and $\mathcal{F}_2^{N_r}$ to maximize SNR_{rx} [22]. Clearly, SNR_{rx} is maximized with $\|\mathbf{f}_{opt}\|_2 = 1$, otherwise energy is unused in beamforming. Further, a simple application of the Cauchy-Schwarz inequality shows that [22] $\mathbf{g}_{opt}$ is a matched filter combiner at the receiver and assuming that $\|\mathbf{g}_{opt}\|_2 = 1$ (for convenience), we obtain $\mathrm{SNR}_{rx} = \rho_f \cdot \mathbf{f}_{opt}^H \mathbf{H}^H \mathbf{H} \mathbf{f}_{opt}$. We thus have

$$\mathbf{f}_{opt} = \mathbf{v}_1, \quad \mathbf{g}_{opt} = \frac{\mathbf{H}\mathbf{v}_1}{\|\mathbf{H}\mathbf{v}_1\|_2}, \tag{7}$$

where $\mathbf{v}_1$ denotes a dominant unit-norm right singular vector (RSV) of H. Here, the singular value decomposition of H is given as $\mathbf{H} = \mathbf{U}\Lambda\mathbf{V}^H$ with U and V being $N_r \times N_r$ and $N_t \times N_t$ unitary matrices of left and right singular vectors, respectively, and arranged so that the corresponding leading diagonal entries of the $N_r \times N_t$ singular value matrix Λ are in non-increasing order.

The following result establishes the connection between the physical directions $\{\phi_{R,\ell}, \phi_{T,\ell}\}$ in the ULA channel model in (3) and $\{\mathbf{f}_{opt}, \mathbf{g}_{opt}\}$ in (7) and confirms the observations in many recent works [14], [23].

Theorem 1: With $\mathbf{H} = H$ and the channel model in (3), all the eigenvectors of $\mathbf{H}^H\mathbf{H}$ can be represented as linear combinations of $\mathbf{v}_1, \cdots, \mathbf{v}_L$ (the transmit array steering vectors). Thus,

---

[8]Consider the following back-of-the-envelope calculation. Let us assume a nominal path loss corresponding to a 100–200 m cell-radius of 130 dB, and mmW-specific shadowing and other losses of 20 dB. We assume a bandwidth of 500 MHz with a noise figure of 7 dB to result in a thermal noise floor of -80 dBm. With an equivalent isotropically radiated power (EIRP) of 40 to 55 dBm in an $N_t = 64$ antenna setting, the pre-beamforming SNR corresponding to 64-level time-repetition (processing) gain (of 18 dB) is -30 to -15 dB. This suggests that low pre-beamforming SNRs are the norm in mmW systems.

$\mathbf{f}_{\text{opt}}$ is a linear combination of $\mathbf{v}_1, \cdots, \mathbf{v}_L$ and $\mathbf{g}_{\text{opt}}$ is a linear combination of $\mathbf{u}_1, \cdots, \mathbf{u}_L$.

Proof: See Appendix A. ∎

Theorem 1 suggests the efficacy of directional beamforming when the channels are sparse [14], [18]–[21], as is likely the case in mmW systems. On the other hand, limited feedback schemes commonly used at cellular frequencies [31]–[33] for CSI acquisition are similar in spirit to directional beamforming schemes for mmW systems. In particular, the typically non-sparse nature of channels at cellular frequencies (corresponding to a large number of paths) washes away any of the underlying Fourier structure [19] of the steering vectors with a uniformly-spaced array. Without any specific structure on the space of optimal beamforming vectors, a good limited feedback code-book such as a Grassmannian line packing solution uniformly quantizes the space of all beamforming vectors.

On a technical note, Theorem 1 provides a non-unitary basis[9] for the eigen-space of $\mathbf{H}^H\mathbf{H}$ (with eigenvalues greater than 0) when $L \le N_t$ (in the $L > N_t$ case, $\{\mathbf{v}_1, \cdots, \mathbf{v}_L\}$ span the eigen-space but do not form a basis). The intuitive meaning of $\mathbf{f}_{\text{opt}}$ and $\mathbf{g}_{\text{opt}}$ is that they perform "coherent" beam-combining by appropriate phase compensation to maximize the energy delivered to the receiver. As an illustration of Theorem 1, in the special case of $L = 2$ paths, when $\mathbf{v}_1$ and $\mathbf{v}_2$ are orthogonal ($\mathbf{v}_1^H\mathbf{v}_2 = 0$), the non-unit-norm version of $\mathbf{f}_{\text{opt}}$ and $\mathbf{g}_{\text{opt}}$ are given as

$$\mathbf{f}_{\text{opt}} = \beta_{\text{opt}} \cdot \mathbf{v}_1 + e^{j\left(\angle\alpha_1 - \angle\alpha_2 - \angle\mathbf{u}_1^H\mathbf{u}_2\right)}\sqrt{1 - \beta_{\text{opt}}^2} \cdot \mathbf{v}_2 \quad (8)$$

$$\mathbf{g}_{\text{opt}} = \alpha_1\beta_{\text{opt}} \cdot \mathbf{u}_1 + e^{j\left(\angle\alpha_1 - \angle\alpha_2 - \angle\mathbf{u}_1^H\mathbf{u}_2\right)}\alpha_2\sqrt{1 - \beta_{\text{opt}}^2} \cdot \mathbf{u}_2 \quad (9)$$

where

$$\beta_{\text{opt}}^2 = \frac{1}{2} \cdot \left[1 + \frac{|\alpha_1|^2 - |\alpha_2|^2}{\sqrt{(|\alpha_1|^2 - |\alpha_2|^2)^2 + 4|\alpha_1|^2|\alpha_2|^2 \cdot |\mathbf{u}_1^H\mathbf{u}_2|^2}}\right]. \quad (10)$$

In addition, if $\mathbf{u}_1$ and $\mathbf{u}_2$ are orthogonal, it can be seen that β_{opt} is either 1 or 0 with full power allocated to the dominant path. At the other extreme of near-parallel $\mathbf{u}_1$ and $\mathbf{u}_2$, the optimal scheme converges to proportional power allocation. That is,

$$\left|\mathbf{u}_1^H\mathbf{u}_2\right| \to 1 \implies \beta_{\text{opt}}^2 \to \frac{|\alpha_1|^2}{|\alpha_1|^2 + |\alpha_2|^2}. \quad (11)$$

If $\mathbf{u}_1$ and $\mathbf{u}_2$ are orthogonal ($\mathbf{u}_1^H\mathbf{u}_2 = 0$), the non-unit-norm version of $\mathbf{f}_{\text{opt}}$ and $\mathbf{g}_{\text{opt}}$ are given as

$$\mathbf{f}_{\text{opt}} = \beta_{\text{opt}} \cdot \mathbf{v}_1 + e^{-j\angle\mathbf{v}_1^H\mathbf{v}_2}\sqrt{1 - \beta_{\text{opt}}^2} \cdot \mathbf{v}_2 \quad (12)$$

$$\mathbf{g}_{\text{opt}} = \alpha_1\left(\beta_{\text{opt}} + |\mathbf{v}_1^H\mathbf{v}_2|\sqrt{1 - \beta_{\text{opt}}^2}\right) \cdot \mathbf{u}_1$$
$$+ e^{-j\angle\mathbf{v}_1^H\mathbf{v}_2}\alpha_2\left(|\mathbf{v}_1^H\mathbf{v}_2|\beta_{\text{opt}} + \sqrt{1 - \beta_{\text{opt}}^2}\right) \cdot \mathbf{u}_2 \quad (13)$$

[9]The use of non-unitary bases in the context of MIMO system studies is not new; see, e.g., [42], [43].

where

$$\beta_{\text{opt}}^2 = \begin{cases} \dfrac{\mathcal{A} + \sqrt{\mathcal{B}}}{2\mathcal{C}} & \text{if } |\alpha_1| \ge |\alpha_2| \\[2mm] \dfrac{\mathcal{A} - \sqrt{\mathcal{B}}}{2\mathcal{C}} & \text{if } |\alpha_1| < |\alpha_2| \end{cases} \quad \text{with}$$

$$\mathcal{A} = \frac{\left(|\alpha_1|^2 - |\alpha_2|^2\right)^2}{|\mathbf{v}_1^H\mathbf{v}_2|^2} + 2|\alpha_1|^2 \cdot \left(|\alpha_1|^2 + |\alpha_2|^2\right) \quad (14)$$

$$\mathcal{B} = \frac{\left(|\alpha_1|^2 - |\alpha_2|^2\right)^4}{|\mathbf{v}_1^H\mathbf{v}_2|^4} + \frac{4|\alpha_1|^2|\alpha_2|^2}{|\mathbf{v}_1^H\mathbf{v}_2|^2} \cdot \left(|\alpha_1|^2 - |\alpha_2|^2\right)^2 \quad (15)$$

$$\mathcal{C} = \left(1 + \frac{1}{|\mathbf{v}_1^H\mathbf{v}_2|^2}\right) \cdot \left(|\alpha_1|^2 + |\alpha_2|^2\right)^2 - \frac{4|\alpha_1|^2|\alpha_2|^2}{|\mathbf{v}_1^H\mathbf{v}_2|^2}. \quad (16)$$

For specific examples, note that β_{opt} converges to 1 or 0 as $\mathbf{v}_1$ and $\mathbf{v}_2$ become more orthogonal. On the other hand, the optimal scheme converges to proportional squared power allocation as $\mathbf{v}_1$ and $\mathbf{v}_2$ become more parallel. That is,

$$|\mathbf{v}_1^H\mathbf{v}_2| \to 1 \implies \beta_{\text{opt}}^2 \to \frac{|\alpha_1|^4}{|\alpha_1|^4 + |\alpha_2|^4}. \quad (17)$$

Similar expressions can be found in [44] for the cases where $\mathbf{v}_1$ and $\mathbf{v}_2$ are near-parallel ($\mathbf{v}_1^H\mathbf{v}_2 \approx 1$), $\mathbf{u}_1$ and $\mathbf{u}_2$ are near-parallel ($\mathbf{u}_1^H\mathbf{u}_2 \approx 1$), etc.

B. Optimal Beamforming With Phase-Only Control

In practice, the antenna arrays at the MWB and UE ends are often controlled by a common PA disallowing per-antenna power control. Thus, there is a need to understand the performance with phase-only control at both the ends. Let $\mathcal{F}_{\infty}^{N_t}$ denote the class of amplitude-constrained beamforming vectors with phase-only control reflecting such an assumption. That is, $\mathcal{F}_{\infty}^{N_t} \triangleq \{\mathbf{f} \in \mathbb{C}^{N_t} : \|\mathbf{f}\|_{\infty} \le \frac{1}{\sqrt{N_t}}\}$. We now consider the problem of optimal beamforming with $\mathbf{f} \in \mathcal{F}_{\infty}^{N_t}$ and $\mathbf{g} \in \mathcal{F}_{\infty}^{N_r}$. Note that if $\mathbf{f} \in \mathcal{F}_{\infty}^{N_t}$, then $\mathbf{f} \in \mathcal{F}_2^{N_t}$. However, unlike the optimization over $\mathcal{F}_2^{N_t}$, it is not clear that the received SNR is maximized by a choice $\mathbf{f}_{\text{opt}}$ with $\|\mathbf{f}_{\text{opt}}\|_{\infty} = \frac{1}{\sqrt{N_t}}$. Nor is it clear that $\|\mathbf{f}_{\text{opt}}\|_2 = 1$. With this background, we have the following result.

Theorem 2: The optimal choice $\mathbf{f}_{\text{opt}}$ from $\mathcal{F}_{\infty}^{N_t}$ is an equal gain transmission scheme. That is, $|\mathbf{f}_{\text{opt}}(i)| = \frac{1}{\sqrt{N_t}}, i = 1, \ldots, N_t$. The optimal choice $\mathbf{g}_{\text{opt}}$ from $\mathcal{F}_{\infty}^{N_r}$ satisfies

$$\mathbf{g}_{\text{opt}} = \frac{1}{\sqrt{N_r}} \cdot \frac{\mathbf{H}\mathbf{f}_{\text{opt}}}{\|\mathbf{H}\mathbf{f}_{\text{opt}}\|_{\infty}}. \quad (18)$$

Proof: See Appendix B. ∎

Note that as with the proof of the optimal beamforming structure from $\mathcal{F}_2^{N_t}$ and $\mathcal{F}_2^{N_r}$ where given a fixed $\mathbf{f} \in \mathcal{F}_2^{N_t}$, the matched filter combiner corresponding to it is optimal from $\mathcal{F}_2^{N_r}$, the matched filter combiner structure in (18) is optimal for any fixed $\mathbf{f} \in \mathcal{F}_{\infty}^{N_t}$. Further, (by construction), $\mathbf{f}_{\text{opt}}$ corresponds to an equal gain transmission scheme, which is also power efficient. That is, $\|\mathbf{f}_{\text{opt}}\|_2 = 1$ and $\|\mathbf{f}_{\text{opt}}\|_{\infty} = \frac{1}{\sqrt{N_t}}$. On the other
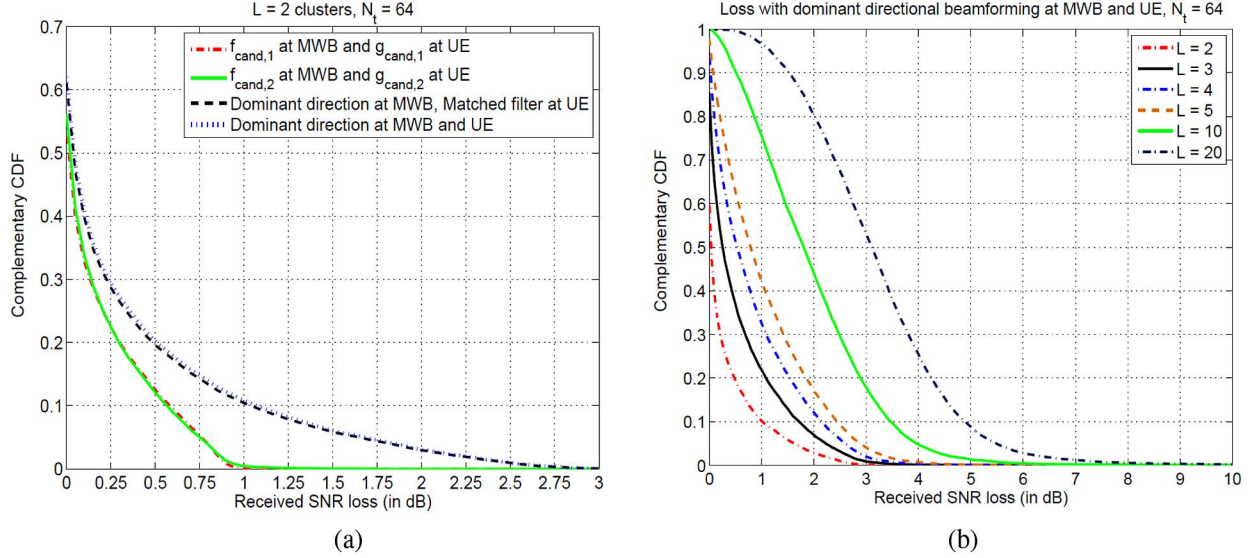
Fig. 1. Complementary CDF of loss in $\mathrm{SNR_{rx}}$ between the optimal beamforming scheme from $\mathcal{F}_2^{N_t}$ in (7) relative to: (a) different beamforming solutions with $L = 2$ clusters, and (b) a dominant directional beamforming scheme with different choices of L.

hand, while $\|\mathbf{g}_{\mathrm{opt}}\|_\infty = \frac{1}{\sqrt{N_r}}$, it is unclear if $\mathbf{g}_{\mathrm{opt}}$ corresponds to an equal gain reception scheme, let alone a power efficient scheme. That is, not only can $\|\mathbf{g}_{\mathrm{opt}}\|_2$ be smaller than 1, but also $|\mathbf{g}_{\mathrm{opt}}(i)|$ need not be $\frac{1}{\sqrt{N_r}}$ for some i.

While Theorem 2 specifies the amplitudes of $\{\mathbf{f}_{\mathrm{opt}}(i)\}$, it is unclear on the phases of $\{\mathbf{f}_{\mathrm{opt}}(i)\}$. In general, the search for the optimal phases of $\mathbf{f}_{\mathrm{opt}}(i)$ appears to be a quadratic programming problem with attendant issues on initialization and convergence to local optima. We now provide two good solutions (as evidenced by their performance relative to the optimal scheme from Sec. III-A in subsequent numerical studies) to the received SNR maximization problem from $\mathcal{F}_\infty^{N_t}$ and $\mathcal{F}_\infty^{N_r}$. The first solution is the equal-gain RSV and its matched filter as candidate beamforming vectors at the two ends ($\mathbf{f}_{\mathrm{cand},\,1}$ and $\mathbf{g}_{\mathrm{cand},\,1}$):

$$\mathbf{f}_{\mathrm{cand},\,1}(i) = \frac{1}{\sqrt{N_t}} \cdot \angle \mathrm{v}_1(i), \; \mathbf{g}_{\mathrm{cand},\,1} = \frac{1}{\sqrt{N_r}} \cdot \frac{\mathbf{H}\mathbf{f}_{\mathrm{cand},\,1}}{\|\mathbf{H}\mathbf{f}_{\mathrm{cand},\,1}\|_\infty}. \tag{19}$$

For the second solution, we have the following statement.

Proposition 1: Let H be decomposed along the column vectors as $\mathbf{H} = [\mathbf{h}_1, \cdots, \mathbf{h}_{N_t}]$. With $\theta_1 = 0$, let θ_i be recursively defined as

$$\theta_i = \angle \left(\sum_{k=1}^{i-1} e^{j\theta_k} \cdot \mathbf{h}_i^H \mathbf{h}_k \right). \tag{20}$$

The beamforming vector $\mathbf{f}_{\mathrm{cand},\,2}$ where $\mathbf{f}_{\mathrm{cand},\,2}(i) = \frac{1}{\sqrt{N_t}} \cdot e^{j\theta_i}$ and $\mathbf{g}_{\mathrm{cand},\,2} = \frac{1}{\sqrt{N_t}} \cdot \frac{\mathbf{H}\mathbf{f}_{\mathrm{cand},\,2}}{\|\mathbf{H}\mathbf{f}_{\mathrm{cand},\,2}\|_\infty}$ lead to a good beamforming solution for the problem considered in this section.

Proof: See Appendix C. ∎

The importance of the beamforming structure from Prop. 1 relative to the one in (19) is that while the latter is just a equal-gain quantization of (7) and thus requires the entire H for its design, the former is more transparent in terms of the column vectors of H and can thus be designed via a simple uplink training scheme.

Fig. 1(a) plots the complementary cumulative distribution function (complementary CDF) of the loss in $\mathrm{SNR_{rx}}$ between the optimal beamforming scheme in (7) and four candidate beamforming schemes: i) equal-gain RSV and matched filter scheme from (19), ii) beamforming scheme from Prop. 1, iii) beamforming along the dominant direction at the MWB and the matched filter to the dominant direction at the UE, and iv) beamforming along the dominant directions at the MWB and the UE in a $N_r = 4$, $N_t = 64$ system generated by $L = 2$ clusters whose AoAs/AoDs are independently and identically distributed (i.i.d.) in the 120° field-of-view (coverage area) of the arrays in the azimuth. From this study, we see that the performance of the scheme from Prop. 1 is similar to that from (19), as is the replacement of matched filter at the UE end with the dominant direction.

C. Issues With RSV Learning

The (near-)optimality of the RSV-type solutions from $\mathcal{F}_2^{N_t}$ and $\mathcal{F}_\infty^{N_t}$ suggests that a reasonable approach for beamformer design is to let the MWB and UE learn an approximation to $\mathbf{f}_{\mathrm{opt}}$ and $\mathbf{g}_{\mathrm{opt}}$, respectively. A similar approach is adopted at cellular frequencies under the rubric of limited feedback schemes that approximate the RSV of the channel from a codebook of beamforming vectors. We specialize this approach and elaborate on their appropriateness for mmW systems.

A well-known RSV learning scheme that exploits the time division duplexing(TDD)-reciprocity of the channel H is power iteration [45, Sec. 7.3] which iterates ($i = 0, 1, \ldots$) a randomly initialized beamforming vector ($\mathbf{f}_0$) over the channel as follows:

$$\widetilde{\mathbf{g}}_{i+1} = \sqrt{\rho_{\mathrm{f}}} \cdot \mathbf{H}\mathbf{f}_i + \mathbf{n}_{\mathrm{f},i+1} \tag{21}$$

$$\mathbf{g}_{i+1} = \frac{\widetilde{\mathbf{g}}_{i+1}}{\|\widetilde{\mathbf{g}}_{i+1}\|_2} = \frac{\sqrt{\rho_{\mathrm{f}}} \cdot \mathbf{H}\mathbf{f}_i + \mathbf{n}_{\mathrm{f},i+1}}{\|\sqrt{\rho_{\mathrm{f}}} \cdot \mathbf{H}\mathbf{f}_i + \mathbf{n}_{\mathrm{f},i+1}\|_2} \tag{22}$$
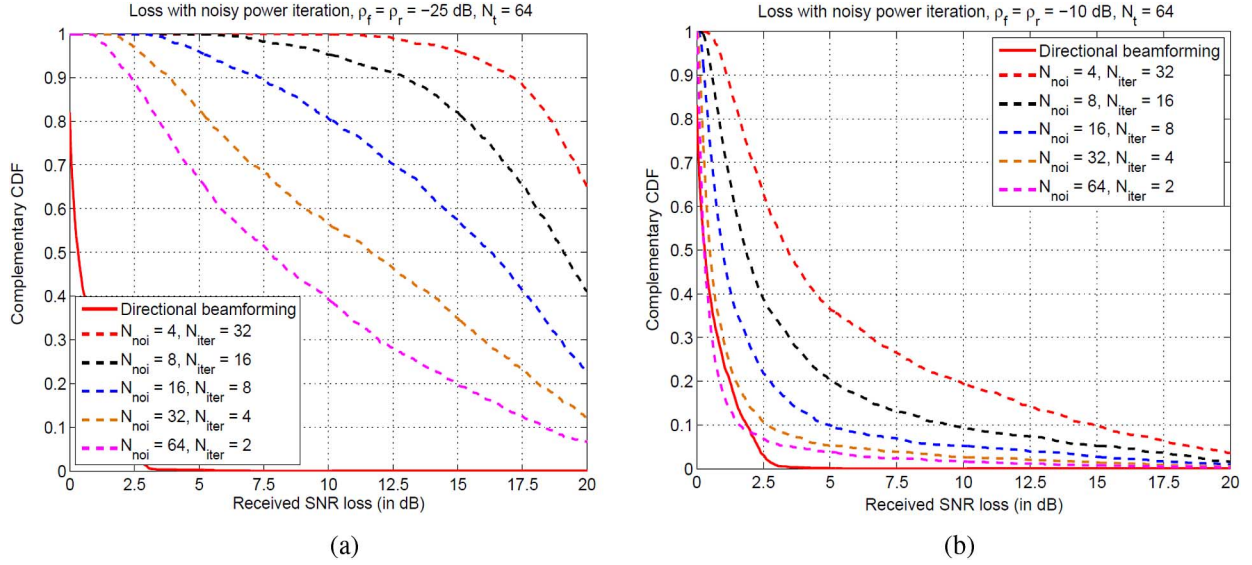
Fig. 2. Complementary CDF of loss in SNR_{rx} between the optimal beamforming scheme from $\mathcal{F}_2^{N_t}$ in (7) and the noisy power iteration scheme with (a) $\rho_{\text{f}} = \rho_{\text{r}} = -25$ dB and (b) $\rho_{\text{f}} = \rho_{\text{r}} = -10$ dB.

$$\mathbf{z}_{i+1} = \sqrt{\rho_{\text{r}}} \cdot \mathbf{H}^T \mathbf{g}_{i+1}^\star + \mathbf{n}_{\text{r},i+1}^\star \qquad (23)$$

$$\mathbf{f}_{i+1} = \frac{\mathbf{z}_{i+1}^\star}{\|\mathbf{z}_{i+1}\|_2} = \frac{\sqrt{\rho_{\text{r}}} \cdot \mathbf{H}^H \mathbf{g}_{i+1} + \mathbf{n}_{\text{r},i+1}}{\|\sqrt{\rho_{\text{r}}} \cdot \mathbf{H}^H \mathbf{g}_{i+1} + \mathbf{n}_{\text{r},i+1}\|_2}. \qquad (24)$$

In (21)–(24), ρ_{f} and ρ_{r} stand for the pre-beamforming SNRs of the forward and reverse links, respectively. A straightforward simplification shows that $\mathbf{f}_{i+1}$ is as in (25) as at the bottom of this page. When the system is noise-free ($\{\rho_{\text{f}}, \rho_{\text{r}}\} \to \infty$), the above algorithm reduces to

$$\mathbf{f}_{i+1} \to \frac{\mathbf{H}^H \mathbf{H} \mathbf{f}_i}{\|\mathbf{H}^H \mathbf{H} \mathbf{f}_i\|_2} \implies \mathbf{f}_{i+1} \to \frac{\left(\mathbf{H}^H \mathbf{H}\right)^{i+1} \mathbf{f}_0}{\|\left(\mathbf{H}^H \mathbf{H}\right)^{i+1} \mathbf{f}_0\|_2} \qquad (26)$$

$$\mathbf{g}_{i+1} \to \frac{\mathbf{H} \mathbf{f}_i}{\|\mathbf{H} \mathbf{f}_i\|_2} \implies \mathbf{g}_{i+1} \to \frac{\mathbf{H} \left(\mathbf{H}^H \mathbf{H}\right)^{i+1} \mathbf{f}_0}{\|\mathbf{H} \left(\mathbf{H}^H \mathbf{H}\right)^{i+1} \mathbf{f}_0\|_2}. \qquad (27)$$

With $\mathbf{H}^H \mathbf{H} = \mathbf{V} \Lambda \mathbf{V}^H$, we have

$$\mathbf{f}_{i+1} = \frac{\sum_{j=1}^{N_t} \mathbf{v}_j \cdot \left(\mathbf{v}_j^H \mathbf{f}_0\right) \cdot \left(\Lambda_j\right)^{i+1}}{\|\sum_{j=1}^{N_t} \mathbf{v}_j \cdot \left(\mathbf{v}_j^H \mathbf{f}_0\right) \cdot \left(\Lambda_j\right)^{i+1}\|_2}. \qquad (28)$$

While the noise-free power iteration scheme has been proposed in the MIMO context in [26], understanding the performance tradeoff of the noisy case analytically appears to be a difficult problem, in general. To surmount this difficulty, we numerically study the performance of the noisy case at a low pre-beamforming SNR on the order of -25 to -10 dB. We consider the case where $N_{\text{npi}} = 256$ samples are used for RSV learning and these samples are partitioned in different ways[10] as $N_{\text{npi}} = 2 N_{\text{noi}} \times N_{\text{iter}}$. Here, N_{noi} samples are

used to improve ρ_{f} by noise averaging and N_{iter} samples are used for beamformer iteration. In particular, we consider the following choices for N_{noi} in our study: $\{4, 8, 16, 32, 64\}$ with $\rho_{\text{f}} = \rho_{\text{r}} = \{-25, -10\}$ dB and Figs. 2(a)-(b) plot the complementary CDF of the loss in SNR_{rx} for these two scenarios in a $L = 2$, $N_r = 4$ and $N_t = 64$ system with averaging over the random choice of $\mathbf{f}_0$. From these two plots, we observe that given N_{npi} samples, noise averaging is a task of higher importance at low pre-beamforming SNRs than beamformer iteration. Nevertheless, in spite of the best noise averaging, the noisy power iteration scheme has a poor performance at low SNRs (for a large fraction of the users at -25 dB and a good fraction at -10 dB) as noise is amplified in the iteration process rather than the channel's RSV.

The RSV learning scheme also suffers from other problems that make its applicability in mmW systems difficult. Since each user's RSV has to be learned via a bi-directional iteration, it is not amenable (in this form) as a common broadcast solution for the downlink setting. This is particularly disadvantageous and impractical if each MWB has to initiate a unicast session with a UE that is yet to be discovered. Further, the need to sample each antenna individually (at both ends) can considerably slow down the iteration process with RF hardware constraints (e.g., when there are fewer RF chains than antennas). In addition, this approach requires calibration of the receive-side RF chain relative to the transmit-side RF chain with respect to phase and amplitude as well as phase coherence during the iteration. More importantly, this approach critically depends on TDD reciprocity, which could be complicated in certain deployment scenarios that do not allow this possibility [9].

An alternate approach given the RSV structure in Theorem 1 is to learn the dominant directions at the MWB end $\{\widehat{\phi}_{\text{T},\ell}\}$ and

---

[10]Note that the 2 factor in the partition of N_{npi} arises because power iteration is bi-directional.

$$\mathbf{f}_{i+1} = \frac{\sqrt{\rho_{\text{f}} \rho_{\text{r}}} \cdot \mathbf{H}^H \mathbf{H} \mathbf{f}_i + \sqrt{\rho_{\text{r}}} \mathbf{H}^H \mathbf{n}_{\text{f},i+1} + \|\sqrt{\rho_{\text{f}}} \mathbf{H} \mathbf{f}_i + \mathbf{n}_{\text{f},i+1}\|_2 \cdot \mathbf{n}_{\text{r},i+1}}{\|\sqrt{\rho_{\text{f}} \rho_{\text{r}}} \cdot \mathbf{H}^H \mathbf{H} \mathbf{f}_i + \sqrt{\rho_{\text{r}}} \mathbf{H}^H \mathbf{n}_{\text{f},i+1} + \|\sqrt{\rho_{\text{f}}} \mathbf{H} \mathbf{f}_i + \mathbf{n}_{\text{f},i+1}\|_2 \cdot \mathbf{n}_{\text{r},i+1}\|_2}. \qquad (25)$$
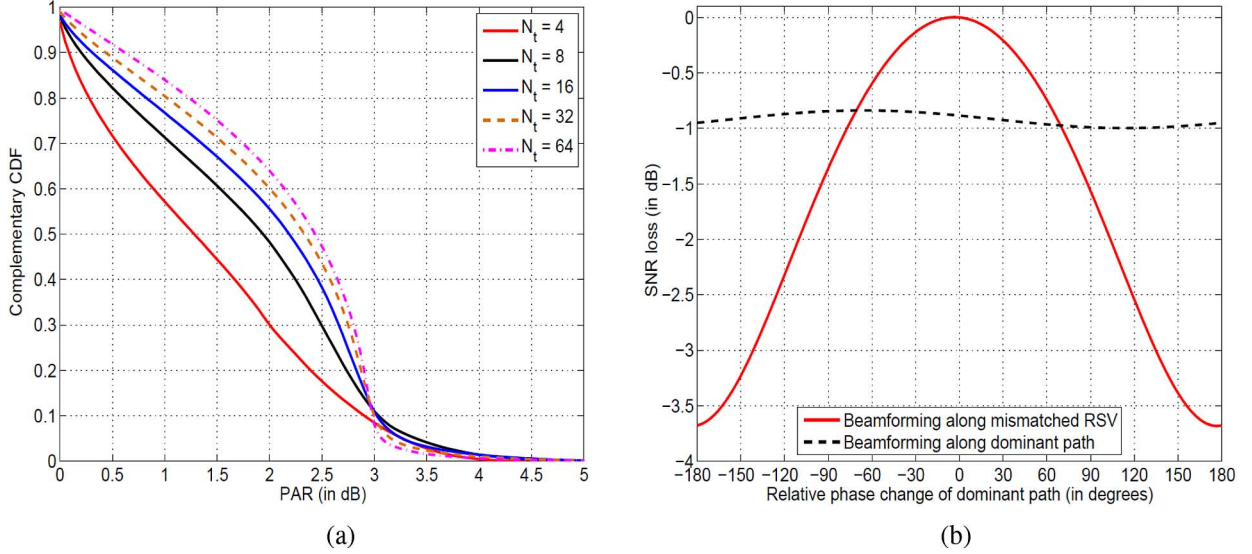
Fig. 3. (a) Complementary CDF of PAR of the combined beamforming vector needed to mimic the RSV structure. (b) Typical performance loss with mismatched RSV and mismatched dominant directional beamforming schemes relative to optimal beamforming in the perturbed case.

then combine the beams with appropriate weights $\{\widehat{\alpha}_\ell\}$ to result in a beamforming vector:

$$\mathbf{f}_{\text{comb}} = \frac{\sum_{\ell=1}^{L} \widehat{\alpha}_\ell \text{CPO}\left(\widehat{\phi}_{\text{T},\ell}\right)}{\left\|\sum_{\ell=1}^{L} \widehat{\alpha}_\ell \text{CPO}\left(\widehat{\phi}_{\text{T},\ell}\right)\right\|_2}. \tag{29}$$

The difficulty with this approach is that it suffers from PA inefficiency (not all the PAs operate at maximal power). Fig. 3(a) plots the complementary CDF of the peak-to-average ratio (PAR) of $\mathbf{f}_{\text{comb}}$, defined as,

$$\text{PAR} \triangleq \frac{\max_i |\mathbf{f}_{\text{comb}}(i)|^2}{1/N_t} = N_t \cdot \max_i |\mathbf{f}_{\text{comb}}(i)|^2 \tag{30}$$

corresponding to beam combining along two randomly chosen, but known directions with random weights. Fig. 3(a) shows that a median PAR loss of over 2 dB is seen for $N_t \geq 8$ suggesting that the RSV gain relative to directional beamforming of less than a dB [see Fig. 1(a)] is significantly outweighed by the PA inefficiency. In other words, the SNR_{rx} loss with just selecting the dominant direction at the MWB and the UE ends is far less than the PA backoff due to combining multiple directions at the MWB or the UE.

More generally, any RSV learning scheme is bound to be extremely sensitive[11] to relative phase changes across paths. For example, Fig. 3(b) plots the typical behavior of loss in SNR_{rx} with the mismatched reuse of the optimal beamformer and the dominant directional beamformer (both from the unperturbed case) relative to the optimal beamformer in the perturbed case as the phase of the dominant path in a $L = 2, N_r = 4,$ $N_t = 64$ system changes. In this example, the two paths are such that $\phi_{\text{R},1} = 108.57^\circ$, $\phi_{\text{T},1} = 83.74^\circ$, $\alpha_1 = 2.61$, $\phi_{\text{R},2} = 92.74^\circ$, $\phi_{\text{T},2} = 94.26^\circ$, $\alpha_2 = 1.79$. We note that the RSV scheme takes a steep fall in performance as the phase changes,

whereas the directional scheme remains approximately stable in performance. It is important to note that a 360° change in phase corresponds to a change in path length of λ (a small distance at higher carrier frequencies and hence an increasingly likely possibility). Such a sensitivity for any RSV reconstruction scheme to phase changes renders this approach's utility in the mmW context questionable.

IV. DIRECTIONAL BEAMFORMING AND DIRECTION LEARNING

Instead of the RSV solution, we now consider the performance loss with a low-complexity strategy that beamforms along the dominant direction at the MWB and the UE. From the numerical study in Fig. 1(a), we see that the dominant directional beamforming scheme suffers only a minimal loss relative to even the best scheme from $\mathcal{F}_2^{N_t}$ and $\mathcal{F}_2^{N_r}$ (a median loss of a fraction of a dB and less than a dB even at the 90-th percentile level). Further, Fig. 1(b) plots the complementary CDF of the loss in SNR_{rx} between the optimal scheme in (7) and the dominant directional beamforming scheme with different choices of L: $L = 2, 3, 4, 5, 10$ or 20. From this study, we note that directional beamforming results in less than a dB loss for over 50% of the users for even up to $L = 5$ clusters. Further, directional beamforming results in no more than 2.5 dB loss for even up to 90% of the users. Thus, this study suggests that learning the directions (AoAs/AoDs) along which the UE and MWB should beamform is a useful strategy for initial UE discovery.

A. Learning Dominant Directions via Subspace Methods

AoA/AoD learning with multiple antenna arrays has a long and illustrious history in the signal/array processing literature [30]. In the simplest case of estimating a single unknown source (signal direction) at the UE end with system equation:

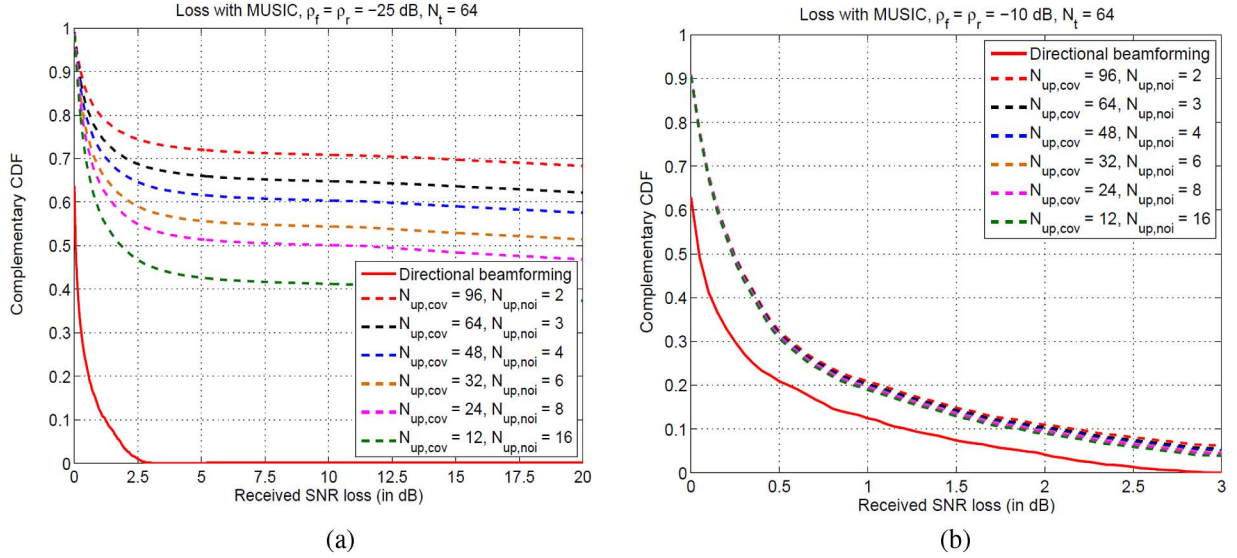$$\mathbf{y} = \alpha_1 \mathbf{u}(\phi_1) + \mathbf{n} \tag{31}$$

---

[11]Note that the higher sensitivity of the eigenvectors of a MIMO channel matrix (relative to the eigenvalues) to small perturbations in the channel entries has been well-understood [46], [47]. See [45, Sec. 7.2] for theoretical details.

Fig. 4. Complementary CDF of loss in $\mathrm{SNR_{rx}}$ between the optimal beamforming scheme in $\mathcal{F}_2^{N_t}$ in (7) and MUSIC with (a) $\rho_f = \rho_r = -25$ dB and (b) $\rho_f = \rho_r = -10$ dB.

where α_1 is known, $\mathbf{u}(\cdot)$ denotes the array steering vector and $\mathbf{n} \sim \mathcal{CN}(\mathbf{0}, \mathbf{I})$, it can be seen that the density function $\log\left(f(\mathbf{y}|\alpha_1, \phi_1)\right)$ can be written as $\mathbf{C} - (\mathbf{y} - \alpha_1\mathbf{u}(\phi_1))^H(\mathbf{y} - \alpha_1\mathbf{u}(\phi_1))$ for an appropriately defined constant C. Thus, the maximum likelihood (ML) solution $(\widehat{\phi}_1)$ that maximizes the density can be seen to be $\widehat{\phi}_1 = \arg\max_\phi |\mathbf{u}(\phi)^H\mathbf{y}|^2$. Rephrasing, correlation of the received vector $\mathbf{y}$ for the best signal strength results in the ML solution for the problem of signal coming from one unknown direction.

In general, if there are multiple (K) sources with system equation

$$\mathbf{y} = \sum_{k=1}^{K} \alpha_k \mathbf{u}(\phi_k) + \mathbf{n}, \qquad (32)$$

the density function of $\mathbf{y}$ is non-convex in the parameters resulting in a numerical multi-dimensional search in the parameter space. In this context, the main premise behind the MUSIC algorithm [28] is that the signal subspace is K-dimensional and is orthogonal to the noise subspace. Furthermore, the K largest eigenvalues of the estimated received covariance matrix, $\widehat{\mathbf{R}}_\mathbf{y}$, correspond to the signal subspace and the other eigenvalues to the noise subspace (provided the covariance matrix estimate is reliable). The MUSIC algorithm then estimates the signal directions by finding the (K) peaks of the pseudospectrum[12], defined as,

$$P_{\mathrm{MUSIC}}(\phi) \triangleq \frac{1}{\sum_{n=K+1}^{N_r} |\mathbf{u}(\phi)^H\widehat{\mathbf{q}}_n|^2} \qquad (33)$$

where $\{\widehat{\mathbf{q}}_{K+1}, \cdots, \widehat{\mathbf{q}}_{N_r}\}$ denote the eigenvectors of the noise subspace of $\widehat{\mathbf{R}}_\mathbf{y}$. The principal advantage of the MUSIC algorithm is that the signal maximization task has been recast as a noise minimization task, a one-dimensional line search problem albeit at the cost of computing the eigenvectors of

$\widehat{\mathbf{R}}_\mathbf{y}$. Nevertheless, since $\{\widehat{\mathbf{q}}_1, \cdots, \widehat{\mathbf{q}}_{N_r}\}$ can be chosen to form a unitary basis, it is seen that MUSIC attempts to maximize $\sum_{n=1}^{K} |\mathbf{u}(\phi)^H\widehat{\mathbf{q}}_n|^2$ (or in other words, it assigns equal weights to all the components of the signal subspace and is hence not ML-optimal).

We now apply the MUSIC algorithm to direction learning at the MWB and UE by a bi-directional approach where the MWB learns the AoD by estimating the uplink covariance matrix (where the UE trains the MWB), and the UE learns the AoA by estimating the downlink covariance matrix (where the MWB trains the UE). We consider the case where $N_\mathrm{music} = 256$ samples are used for direction learning. Since the MWB is equipped with more antennas than the UE, we partition N_music into $N_\mathrm{up} = 192$ samples for uplink (AoD) training and $N_\mathrm{down} = 64$ samples for downlink (AoA) training. As before, we partition N_up in different ways as $N_\mathrm{up} = N_\mathrm{up,cov} \times N_\mathrm{up,noi}$ where $N_\mathrm{up,noi}$ samples are used for link margin improvement and $N_\mathrm{up,cov}$ samples are used for uplink covariance matrix estimation. In particular, we study the following choices here: $N_\mathrm{up,cov} = \{12, 24, 32, 48, 64, 96\}$. $N_\mathrm{down} = 64$ is partitioned as $N_\mathrm{down,noi} = N_\mathrm{down,cov} = 8$. Figs. 4(a) and (b) plot the complementary CDF of $\mathrm{SNR_{rx}}$ with such a bi-directional MUSIC algorithm for $\rho_f = \rho_r = -25$ dB and -10 dB, respectively. In general, $\rho_f > \rho_r$ and Fig. 4 serves as a more optimistic characterization of the MUSIC scheme for mmW systems.

From Fig. 4, we note that the performance is rather poor at low link margins, but significantly better as the link margin improves. An important reason for the poor performance of the MUSIC approach is that consistent covariance matrix estimation becomes a difficult exercise with very few samples, especially as the antenna dimensions increase at the MWB end. Furthermore, as with the noisy power iteration scheme, MUSIC also requires a non-broadcast system design. It also suffers from a high computational complexity (dominated by the eigen-decomposition of an $N_t \times N_t$ matrix in uplink training). In general, the computational complexity of MUSIC can be traded off by constraining the antenna array structure in various

---

[12]In general, the choice of K in (33) has to be estimated via an information theoretic criterion as in [48] or via minimum description length criteria such as those due to Rissanen or Schwartz.
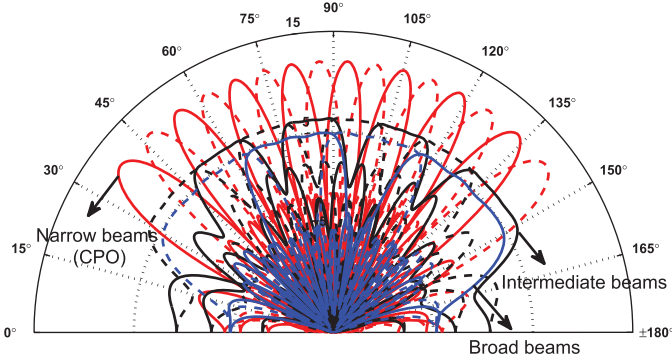
Fig. 5. Main idea of beam broadening illustrated with the overlaid beam patterns of beamforming vectors from three (narrow/CPO beams, intermediate beams and broad beams) codebooks.

ways. Nevertheless, we expect the computational complexity of other such constrained AoA/AoD learning techniques such as Estimation of Signal Parameters via Rotational Invariance Techniques (ESPRIT) algorithm [29], Space-Alternating Generalized Expectation maximization (SAGE) algorithm [49], [50], higher-order singular value decomposition, RIMAX [51], and compressive sensing techniques that employ nuclear norm optimization [52]–[54] to be of similar nature as the MUSIC algorithm. All these reasons suggest that while the MUSIC algorithm may be useful for beam refinement after the UE has been discovered, its utility in UE discovery is questionable.

B. Beam Broadening for Initial UE Discovery

Let Ω denote the beamspace transformation at the MWB side, $\Omega = kd_{\mathrm{T}}\cos(\phi_{\mathrm{T}}) = \pi\cos(\phi_{\mathrm{T}})$, corresponding to an inter-antenna spacing of $\lambda/2$. Towards the goal of alternate direction learning strategies, we consider the problem of understanding the tradeoff in the design of beamforming vectors that cover a beamspace area of $\overline{\Omega}$ with as few beamforming vectors as possible without sacrificing the worst-case beamforming gain in the coverage area [15], [34].

The basic idea of beam broadening is illustrated in Fig. 5 where three different codebooks of beamforming vectors are used to cover a coverage area of 120° (from 30° to 150°). The first codebook (illustrated in red) consists of narrow CPO beams (pointing at optimally chosen directions over the coverage area) which leads to a peak beamforming gain of $10\log_{10}(N_t)$ dB as well as a reasonably high worst-case beamforming gain over the coverage area, although at the cost of a high UE discovery latency corresponding to a beam sweep over 16 directions/beams. The second codebook (illustrated in black) consists of intermediate beams which leads to a lower peak beamforming gain (as well as a worst-case gain) over the coverage area, but the UE discovery period is shortened as it now consists of a beam sweep over 8 directions/beams. The third codebook (illustrated in blue) consists of broad beams which

leads to a more reduced peak beamforming gain, but the UE discovery period is a sweep over only 4 directions/beams. Either codebook could be useful for initial UE discovery depending on the link margin of the UE's involved. For example, a UE geographically close to the MWB and suffering minimal path loss can accommodate a broad beam codebook and be quickly discovered, whereas a UE at the cell-edge or suffering from huge blocking losses may need the narrow CPO beam codebook to even close the link with the MWB. The intermediate codebook trades off these two properties.

We now recast the above idea in the form of a well-posed optimization problem. For this, given a beamspace coverage area of Ω_0 for a single beam (centered around $\Omega_{\mathrm{c}} = \pi/2$, without loss in generality), we seek the design of:

$$\mathbf{f}_{\Omega_0} \triangleq \arg \max_{\mathbf{f}\in\mathcal{F}_\infty^{N_t}} \min_{\Omega\in\left[\Omega_{\mathrm{c}}-\frac{\Omega_0}{2},\Omega_{\mathrm{c}}+\frac{\Omega_0}{2}\right]} |\mathbf{F}(\Omega)|^2 \quad (34)$$

where $\mathbf{F}(\Omega) = \sum_{n=0}^{N_t-1}\mathbf{f}(n)e^{-j\Omega n} = \mathbf{a}(\Omega)^H\mathbf{f}$ with $\mathbf{a}(\Omega) = \left[1, e^{j\Omega}, \ldots, e^{j(N_t-1)\Omega}\right]^T$. With $\mathbf{f}_{\Omega_0}$ as template, the number of beamforming vectors needed to cover $\overline{\Omega}$ (say, a 120° field-of-view as in Fig. 5 is No. beams $= \frac{\overline{\Omega}}{\Omega_0}$.

We start with an upper bound on the tradeoff between No. beams and the worst-case beamforming gain over $\overline{\Omega}$. From the Parseval identity, we have the following trivial relationship for any $\mathbf{f}$:

$$\frac{1}{2\pi}\int_{-\pi}^{\pi}|\mathbf{F}(\Omega)|^2 d\Omega = \sum_{n=0}^{N_t-1}|\mathbf{f}(n)|^2 \leq 1. \quad (35)$$

If $\min_{\Omega\in\left[\Omega_{\mathrm{c}}-\frac{\Omega_0}{2},\Omega_{\mathrm{c}}+\frac{\Omega_0}{2}\right]}|\mathbf{F}(\Omega)|^2 = P$, we have the chain of inequalities as in (36) as at the bottom of this page. Further, P is also constrained as $P \leq N_t$ since the maximal beamforming gain cannot exceed N_t in any direction. Thus, the worst-case beamforming gain over this area (in dB) is upper bounded as

$$\text{BF Gain} \triangleq 10\log_{10}(P)$$
$$\leq 10\log_{10}\left(\min\left(N_t, \frac{2\pi}{\overline{\Omega}}\cdot\text{No. beams}\right)\right). \quad (37)$$

We now provide an alternate non-trivial approach based on computation of eigenvalues of certain appropriately-defined matrices for a better upper bound of this tradeoff.

Theorem 3: Let $\Omega_j, j = 1, \cdots, J$ be a set of sampling frequencies over the beamspace area of Ω_0 spanned by the beamforming vector $\mathbf{f}$. The worst-case beamforming gain with $\mathbf{f}$ is upper bounded by the solution to the following optimization:

$$\text{BF Gain} \leq$$
$$10\log_{10}\left(N_t, \min_{J,\{\Omega_j\}}\frac{\lambda_{\max}\left(\sum_{j=1}^{J}\mathbf{a}(\Omega_j)\mathbf{a}(\Omega_j)^H\right)}{J}\right) \quad (38)$$

$$\frac{1}{2\pi}\int_{-\pi}^{\pi}|\mathbf{F}(\Omega)|^2 d\Omega \geq \frac{1}{2\pi}\int_{\Omega\in\left[\Omega_{\mathrm{c}}-\frac{\Omega_0}{2},\Omega_{\mathrm{c}}+\frac{\Omega_0}{2}\right]}|\mathbf{F}(\Omega)|^2 d\Omega \geq P\cdot\frac{\Omega_0}{2\pi} \implies P \leq \frac{2\pi}{\Omega_0}. \quad (36)$$

where $\Omega_j \in \left[\Omega_c - \frac{\Omega_0}{2}, \Omega_c + \frac{\Omega_0}{2}\right]$ with $\Omega_0 = \frac{\overline{\Omega}}{\text{No. beams}}$ and $\lambda_{\max}(\bullet)$ stands for the largest eigenvalue of the underlying positive semi-definite matrix.

Proof: See Appendix D. ∎

Fig. 6(a) numerically optimizes the expression in (38) and plots the upper bound to the worst-case beamforming gain as a function of the number of beams to cover a 120° field-of-view with $N_t = 64$. For the eigenvalue-based approach, we plot the upper bound for specific choices of J with $\{\Omega_j\}$ optimized, as well as the upper bound based on a joint optimization over J and $\{\Omega_j\}$. Note that the horizontal segments in the joint optimization correspond to the fact that the tradeoff with a larger number of beams can be no worse than the tradeoff with a smaller number of beams.

In contrast to the upper bound, we now propose specific approaches towards the goal of beam broadening. For this, we initially consider partitioning of the antenna array at the MWB side into *virtual subarrays* where each virtual subarray is used to beamform to a certain appropriately-chosen virtual direction. The expectation from this approach is that the beam patterns from the individual virtual subarrays combine to enhance the coverage area of the resultant beam with minimal loss in peak gain due to reduction in the effective aperture of the subarrays.

As a specific example, in the $M = 2$ virtual subarray setting, we propose the following beamforming vector that orients along $\pi - \cos^{-1}\left(\frac{2f}{N_t}\right)$ and $\cos^{-1}\left(\frac{2f}{N_t}\right)$ with each half of the array. That is, $\mathbf{f}$ as in (39) at the bottom of this page is designed to be a broadened beam by optimally choosing f. Similarly, in the $M = 3$ and $M = 4$ settings, we propose the beamforming vectors in (40) and (41), both at the bottom of this page, with two parameters (f and $0 \le L \le \frac{N_t}{2}$) and three parameters (f, δf and $0 \le L \le \frac{N_t}{2}$), respectively. Note that (40) reduces to

the $M = 2$ setting in (39) with $L = 0$ where the beams are pointed at f, and with $L = \frac{N_t}{2}$ where the beams are pointed at f = 0. Similarly, (41) reduces to the $M = 2$ setting with $L = 0$ and $L = \frac{N_t}{2}$ where the beams are pointed at f + δf and f, respectively.

Fig. 6(b) plots the optimal values of f (and δf) designed to maximize $\min |\mathbf{F}(\Omega)|^2$ as a function of Ω_0 with $M = 2, 3, 4$ and $N_t = 64$. Fig. 6(c) plots the length of the middle subarray in the $M = 3$ case (middle subarrays in the $M = 4$ case) as a function of Ω_0. From these two plots, we see that for small values of Ω_0, choosing f = 0 is optimal, whereas the length of the middle subarray decreases as Ω_0 increases corresponding to gradual beam orientation away from f = 0. Fig. 6(d) plots the shape of the broadened beams so optimized for three choices of Ω_0: $\frac{\Omega_0}{2\pi/N_t} = \{1.3, 2, 3.5\}$. Also, plotted are vertical lines at $\frac{\Omega_0}{2\pi/N_t} = \pm 1.3, \pm 2, \pm 3.5$. From this plot, we see that within their corresponding regimes, each broadened beam maximizes $\min |\mathbf{F}(\Omega)|^2$. In addition, Fig. 7(a) captures the tradeoff between the number of beamforming vectors and the worst-case beamforming gain with the $M = 2, 3, 4$ subarray scheme in the $N_t = 64$ case. Clearly, across all regimes of interest of No. beams, the $M = 4$ subarray scheme is within a couple of dB of the upper bound in terms of beamforming gain illustrating the utility of the proposed approach.

C. Learning Dominant Directions via Beam Sweep With Broadened Beam Codebooks

We use the template broadened beamforming vectors designed in Sec. IV-B corresponding to different beam broadening factors (and their shifted versions) to design a beam sweep codebook for the MWB side. In particular, we consider those beam broadening factors that lead to

$$\mathbf{f}(n) = \frac{1}{\sqrt{N_t}}\begin{cases} \exp\left(-\frac{j2\pi f}{N_t}\left(n - \frac{N_t}{2} + \frac{1}{2}\right)\right) & \text{if } 0 \le n \le \frac{N_t}{2} - 1 \\ \exp\left(\frac{j2\pi f}{N_t}\left(n - \frac{N_t}{2} + \frac{1}{2}\right)\right) & \text{if } \frac{N_t}{2} \le n \le N_t - 1 \end{cases} \tag{39}$$

$$\mathbf{f} = \frac{1}{\sqrt{N_t}}\begin{cases} \exp\left(-\frac{j2\pi f}{N_t}\left(n - \frac{N_t}{2} + \frac{1}{2} + L\right)\right) & \text{if } 0 \le n \le \frac{N_t}{2} - L - 1 \\ 1 & \text{if } \frac{N_t}{2} - L \le n \le \frac{N_t}{2} + L - 1 \\ \exp\left(\frac{j2\pi f}{N_t}\left(n - \frac{N_t}{2} + \frac{1}{2} - L\right)\right) & \text{if } \frac{N_t}{2} + L \le n \le N_t - 1, \end{cases} \tag{40}$$

$$\mathbf{f} = \frac{1}{\sqrt{N_t}}\begin{cases} \exp\left(-\frac{j2\pi (f + \delta f)}{N_t}\left(n - \frac{N_t}{2} + \frac{1}{2}\right) - \frac{j2\pi \cdot \delta f}{N_t}\left(L - \frac{1}{2}\right)\right) & \text{if } 0 \le n \le \frac{N_t}{2} - L - 1 \\ \exp\left(-\frac{j2\pi f}{N_t}\left(n - \frac{N_t}{2} + \frac{1}{2}\right)\right) & \text{if } \frac{N_t}{2} - L \le n \le \frac{N_t}{2} - 1 \\ \exp\left(\frac{j2\pi f}{N_t}\left(n - \frac{N_t}{2} + \frac{1}{2}\right)\right) & \text{if } \frac{N_t}{2} \le n \le \frac{N_t}{2} + L - 1 \\ \exp\left(\frac{j2\pi (f + \delta f)}{N_t}\left(n - \frac{N_t}{2} + \frac{1}{2}\right) - \frac{j2\pi \cdot \delta f}{N_t}\left(L - \frac{1}{2}\right)\right) & \text{if } \frac{N_t}{2} + L \le n \le N_t - 1. \end{cases} \tag{41}$$
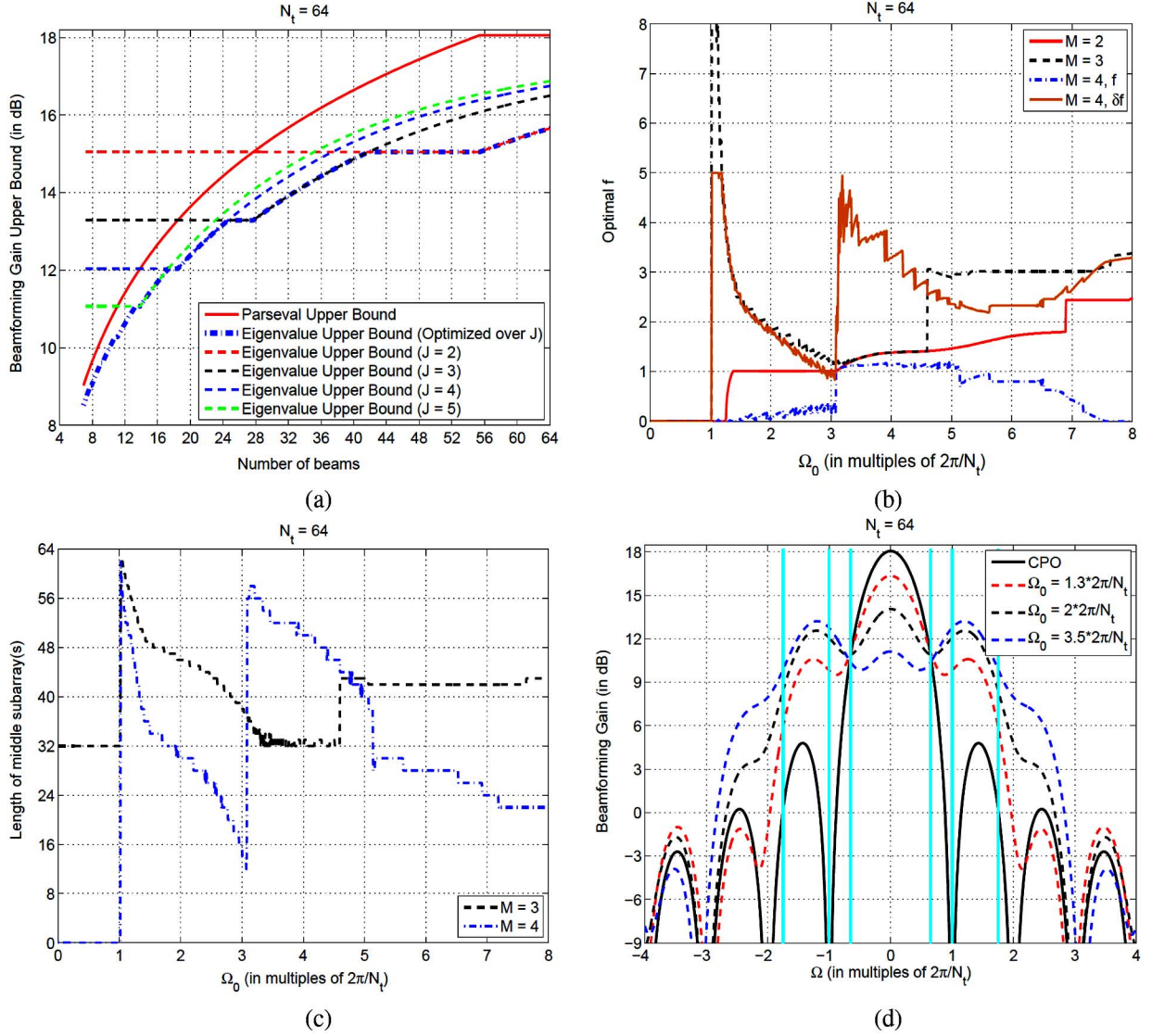
Fig. 6. (a) Upper bound to the beamforming gain vs. number of beams tradeoff for $N_t = 64$. (b) Optimal f and (c) length of middle subarray(s) as a function of Ω_0 for different choices of M. (d) Beam patterns of broadened beams for certain choices of Ω_0 in the $M = 2$ case.

$N_{\mathrm{mwb}} = \{8, 16, 24, 32, 40, 48, 56, 64\}$ elements in the beam sweep codebook at the MWB. On the other hand, since $N_r = 4$ at the UE side, a simpler codebook of $N_{\mathrm{ue}} = 4$ beamforming vectors corresponding to an equal partition of the field-of-view is sufficient for the purpose of beam sweep. With these different codebook choices at the MWB and UE, we find the best choice of beamforming vectors that maximize $\mathrm{SNR_{rx}}$ and use them for subsequent beamforming/beam refinement. An important advantage of the beam sweep approach is that it allows a broadcast solution (the same codebook can be reused across multiple UEs within the field-of-view).

Fig. 7(b) plots the complementary CDF of the loss in $\mathrm{SNR_{rx}}$ with the beam sweep approach at $\rho_f = -10$ dB. Fig. 8(a) compares the complementary CDF of loss in $\mathrm{SNR_{rx}}$ with the best noisy power iteration scheme, MUSIC algorithm and the beam sweep approach at the same ρ_f value. Clearly, the beam sweep approach has a poorer performance relative to the other schemes, but its simplicity results in a better system design than possible with the other approaches. Further,

Fig. 8(b) plots the loss in $\mathrm{SNR_{rx}}$ at different percentile levels $(10\%, 25\%, 50\%, 75\%, 90\%$ and $95\%)$ as a function of the number of samples used in channel learning with the beam sweep scheme. From this study, we note that at small coverage levels, certain codebook size choices are better in the tradeoff curve than other choices (for example, a $N_{\mathrm{mwb}} = 20$ codebook over a $N_{\mathrm{mwb}} = 40$ codebook) and these advantages correspond to the steepness of the achievability curve (see Fig. 7(a)).

Further, while $\mathrm{SNR_{rx}}$ improves as the codebook size increases, good users with a better link margin (e.g., users with a smaller path loss) can be discovered with a lower discovery latency (corresponding to a smaller codebook size) than those cell-edge/blocked users with a worser link margin. Fig. 8(b) suggests a smooth roll-off in the discovery latency of the users with a worser link margin. That said, the beam sweep approach could indeed suffer a significant loss in performance especially with a cell-edge/blocked user. In such scenarios, the design for such a user could include coding over long sequences for enhanced time-repetition/processing gain, high
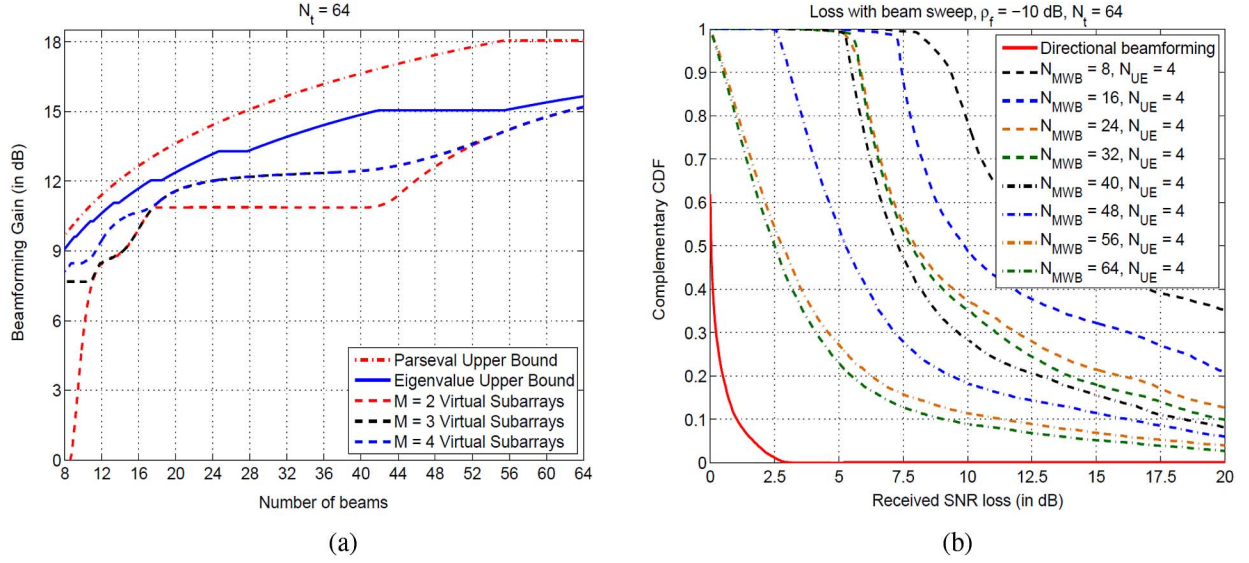
Fig. 7. (a) Performance tradeoff with different beam broadening approaches for $N_t = 64$. (b) Complementary CDF of loss in SNR_{rx} between the optimal beamforming scheme in $\mathcal{F}_2^{N_t}$ in (7) and beam sweep with the broadened beams as in Fig. 7(a) at $\rho_f = -10$ dB.
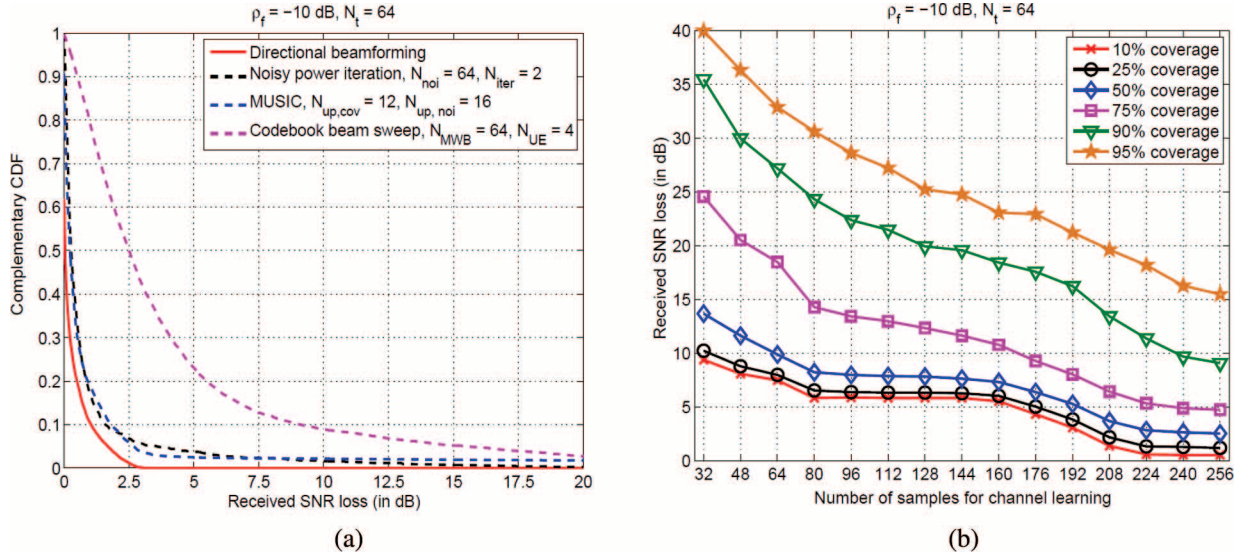

Fig. 8. (a) Comparison of complementary CDF of SNR_{rx} loss with different beamforming approaches at $\rho_f = \rho_r = -10$ dB. (b) Tradeoff between number of samples for channel learning with the beam sweep approach and loss in SNR_{rx} in initial UE discovery.

MWB densification, a low-frequency overlay of multiple narrow CPO beams with a worst-case beamforming gain (as close to the $10 \log_{10}(N_t)$ dB peak gain) in the coverage area, among many approaches. However, such a design could lead to a significant drag on the performance tradeoffs of the good/median user. Thus, they could be initiated by the UE when it perceives a poor link on a unicast basis.

V. COMMENTS ON PRACTICAL APPLICATIONS

A. Finite-Bit Phase Shifters

The entire focus of this work has been on beamformers that can be realized with infinite-precision phase shifters allowing an arbitrary phase resolution for the beamformer weights. However, in practice, beamformers at both the MWB and UE ends are constrained to use finite-bit phase shifters.

Nevertheless, our studies suggest that even a $B = 3$ or $B = 4$ bit phase shifter (which is practically realizable at low cost) is sufficient. Specifically, Fig. 9(a) considers the $L = 2$, $N_r = 4$ and $N_t = 64$ case considered in Fig. 1(a) with $B = 3$ and $B = 4$ bit phase shifters and plots the loss in SNR_{rx} relative to the infinite-precision optimal beamforming scheme. From Fig. 9(a), we observe a minimal loss (less than 0.25 dB) with a $B = 4$ bit phase shifter, thereby suggesting that quantization is not a serious detriment to the performance of mmW MIMO systems. This justifies focus on infinite-precision beamformers in this work.

B. More Antennas at the UE End

A larger number of antenna elements (at the MWB and UE ends) could render mmW systems more attractive in terms of data rates. With this backdrop, the UE-side and MWB-side
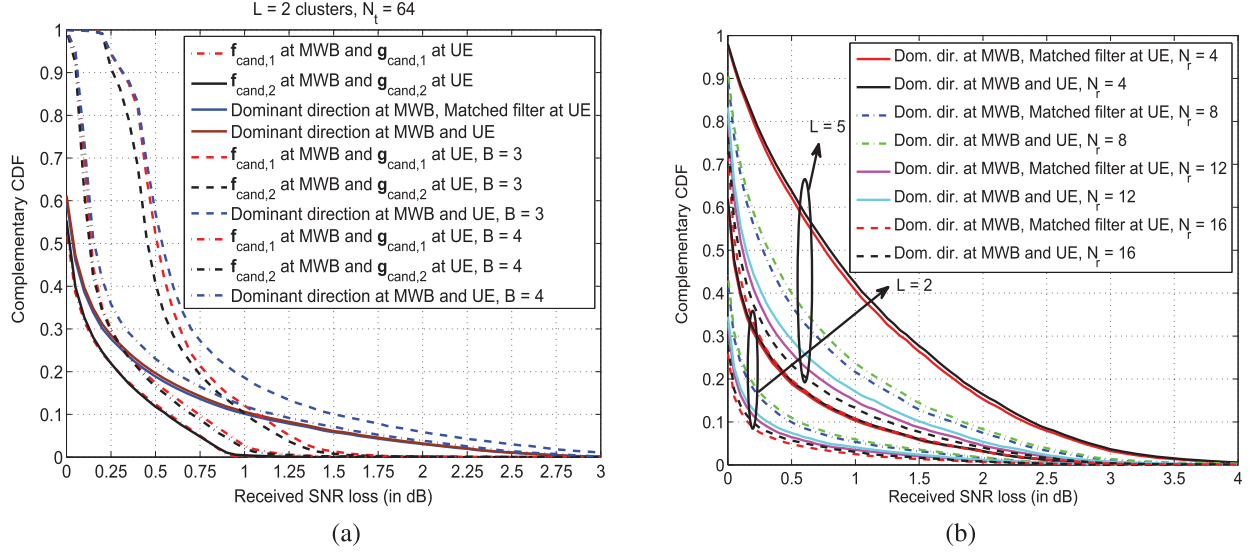
Fig. 9. (a) Loss in SNR_{rx} with different RSV-type beamforming schemes with perfect phase of beamformers, and finite $B = 3$ and $B = 4$ bit phase quantization. (b) Complementary CDF of loss in SNR_{rx} as a function of N_r with $L = 2$ and $L = 5$ clusters.

antenna numbers of $N_r = 4$ and $N_t = 64$ in our simulation studies can be justified as follows. The MWB serves as a network resource with softer constraints on the array aperture and hence, sectorized coverage (90° or 120° coverage per array at the MWB end) is likely leading to a larger number of antennas at this end. On the other hand, multiple subarrays need to deployed at the UE end to cover all the sectors leading to a smaller-dimensional subarray. For example, a 16 element antenna array consisting of 4 subarrays of 4 antennas each with a $\lambda/2$ inter-antenna element spacing would still require an aperture of 7.5 cm at 30 GHz — a considerable expense in array aperture at the UE end. Thus, the $N_r = 4$ assumption made in this work is not conservative, but quite realistic for practical mmW systems.

As N_r increases, the performance of all the directional schemes get better relative to the optimal scheme (this is also true in terms of absolute values of SNR_{rx} due to increased array gain with increasing N_r, but this is not shown here) as can be seen from Fig. 9(b) where the complementary CDF of loss in SNR_{rx} is plotted for the $N_t = 64$ case with $L = 2$ and $L = 5$ clusters for four different choices of N_r: $N_r \in \{4, 8, 12, 16\}$. While these plots correspond to perfect directional beamforming, with reasonable ρ_f, we expect the performance of the directional learning schemes such as beam sweep or MUSIC to get similarly better with increasing N_r.

C. Coherence Time Constraints

In addition to the different architectural tradeoffs in terms of system design, the realizability of different beamforming strategies also critically depend on the coherence time of the mmW channel. Initial measurement studies suggest that the coherence time is on the order of a few milliseconds [27], [55]. While this coherence time is considerably (an order of magnitude) shorter than in sub-6 GHz systems, this constraint only leads to a more favorable view of directional beamforming approaches relative to RSV-type schemes due to the need for a

bi-directional feedback for the implementation of an RSV-type scheme. Fig. 3(b) also addresses the lack of robustness with an RSV-type scheme due to small path length changes that could happen at a sub-coherence time level. On the other hand, the essentially stable performance of the directional beamforming scheme to such changes makes it an attractive candidate for initial UE discovery.

D. Planar Antenna Arrays

While the entire development in this paper so far assumed an ULA geometry for the antennas, this was done primarily for the sake of illustrating the tradeoffs in the beam broadening problem which would have been difficult with a smaller dimensional planar array, e.g., 8×8. More general expressions can be written for the array steering vectors when the antennas are laid out according to other geometric configurations [14], [56]. In particular, the proposed development of this paper can be easily extended to a planar array geometry.

E. Comparison With Other Initial UE Discovery Approaches

Jeong *et al.* [35] study a random access procedure for initial UE discovery based on beam scanning and propose different approaches to enhance the performance of beam sweep such as the use of multiple RF chains, enhanced preamble detection, optimal cell design, etc. However, the viability of beam scanning as a beamforming procedure for initial UE discovery (relative to other signal processing-based techniques) is not considered in [35].

Ghadikolaei *et al.* [36] also address the initial UE discovery problem and characterize the essential tradeoffs in the design of control channels. Initial UE search approaches such as an omni-directional beam sweep, one-sided directional beam sweep, or a bi-directional beam sweep are considered. Since the performance tradeoffs are addressed from a MAC layer perspective, PHY aspects such as beamformer design under RF constraints,

TABLE I
QUALITATIVE COMPARISON BETWEEN DIFFERENT BEAMFORMING APPROACHES

Issue of interest	RSV Learning	MUSIC/ESPRIT	Compressive Sensing	Beam Sweep
Computational complexity	Iterative method	Computing eigenvectors	Convex optimization or similar	Received SNR computation
PAR of beamforming vector	Non-constant amplitude	CPO beam for training	Non-constant amplitude for good dictionary	CPO beam
Performance robustness	Poor	Poor	Reasonable	Reasonable
System design issues	Unicast Bi-directional	Unicast Bi-directional	Broadcast Uni-directional	Broadcast Uni-directional
Scaling with analog beamforming	Poor	Poor	Poor with a general dictionary	Comparable

tradeoffs between and implications of different beamforming approaches on mmW system design, etc. are not considered in [36]. Nevertheless, our work is similar in flavor to [36] in terms of the received SNR vs. initial UE discovery latency tradeoff that both works quantify from PHY and MAC viewpoints, respectively.

The theme considered in Barati *et al.* [37] for the initial UE discovery problem is closely aligned with the theme of our work. The authors consider a beam sweep procedure and derive the structure of generalized likelihood ratio detectors for detecting the primary sync signal. Based on this study, the authors conclude that omni-directional beam scanning provides a better tradeoff point in the received SNR vs. initial UE discovery latency curve than a beam sweep. At this stage, note that an extreme case of beam broadening considered in our work (where only one beam covers the entire coverage area) is equivalent to an omni-directional scan considered in [37] and thus the issue lies in figuring out the best tradeoff point on the received SNR vs. initial UE discovery tradeoff curve. Independent of performance comparisons, from a system design perspective, as the authors rightly point out in [37], detection of the primary sync signal via an omni-directional scan provides no knowledge of the AoD after the detection/discovery of the UE unlike in the beam sweep case (broadened codebooks lead to increasing uncertainty on the AoD that needs to be refined subsequently). For an asymmetric downlink setup (as considered in this work), knowledge of AoD is more important than that of AoA for the subsequent data delivery stage. Thus, it would be of interest in understanding the latency tradeoffs between a broad beam scan (with omni-directional scan as an extreme case) for the initial UE discovery stage followed by beam/AoD refinement for the data delivery stage. While Fig. 8(b) of this work provides a certain preliminary analysis, a more detailed study would be of interest. Furthermore, architecturally speaking, an omni-directional scan would also render the discovery of multiple MWBs impossible. Given that a mmW setup is expected to be primarily of use in a small cell setting with a number of potential MWBs available for handoff, lack of knowledge of AoD in an omni-directional scan could be potentially a disadvantage.

VI. CONCLUDING REMARKS

We studied the efficacy of different beamforming approaches for initial UE discovery in mmW MIMO systems in this work.

The structure of the (near-)optimal beamformers suggested RSV learning as a useful strategy for beamformer learning. However, RSV learning is sensitive to small path length changes, a problem of serious importance at mmW carrier frequencies. A further examination of the beamformer structure suggests direction (AoA/AoD) learning as a viable strategy. We started by studying the utility of classical approaches such as MUSIC in the context of direction learning. As with RSV learning, MUSIC also requires a non-broadcast system design that could render it unattractive from a system level standpoint. An alternate strategy motivated by the limited feedback approach at cellular frequencies (albeit a directional codebook in the mmW context) of SNR estimation via the use of a codebook of beamforming vectors at the MWB and UE is seen to result in a broadcast solution that is conducive for initial UE discovery. While this approach has a slightly poor performance relative to RSV learning and MUSIC, its simplicity outweighs its sub-optimality. Table I provides a brief summary of the features of the different beamforming algorithms such as computational complexity, PAR of beamforming vector, system design issues and scaling with different beamformer architectures.

APPENDIX

A. Proof of Theorem 1

The $N_t \times N_t$ matrix $\mathbf{H}^H\mathbf{H}$ can be expanded as

$$\frac{L}{N_t N_r} \cdot \mathbf{H}^H\mathbf{H} = \sum_{i,j} \alpha_i^\star \alpha_j \cdot \left(\mathbf{u}_i^H \mathbf{u}_j\right) \cdot \mathbf{v}_i \mathbf{v}_j^H = \mathbf{VAV}^H \quad (42)$$

where $\mathbf{V} = [\alpha_1^\star \mathbf{v}_1, \ldots, \alpha_L^\star \mathbf{v}_L]$ and $\mathbf{A}(i,j) = \mathbf{u}_i^H \mathbf{u}_j, i, j = 1, \ldots, L$. Let X be an $L \times L$ eigenvector matrix of $\mathbf{AV}^H\mathbf{V}$ with the corresponding diagonal matrix of eigenvalues denoted by D. That is (the eigenvalue equation is given as),

$$\left(\mathbf{AV}^H\mathbf{V}\right) \cdot \mathbf{X} = \mathbf{X} \cdot \mathbf{D}. \quad (43)$$

Pre-multiplying both sides of (43) by V, we have

$$\mathbf{VX} \cdot \mathbf{D} = \left(\mathbf{VAV}^H\mathbf{V}\right) \cdot \mathbf{X} = \left(\frac{L}{N_t N_r} \cdot \mathbf{H}^H\mathbf{H}\right) \cdot \mathbf{VX}. \quad (44)$$

Reading (44) from right to left, we see that VX forms the eigenvector matrix for $\mathbf{H}^H\mathbf{H}$ with the diagonal eigenvalue matrix being the same as D. In other words, all the eigenvectors

of $H^H H$ (and hence f_{opt}) can be represented as *linear combinations* of $v_1, \ldots, v_L$. The only difference between the $L \leq N_t$ and $L > N_t$ cases is that the number of distinct eigenvectors of X is less than or equal to L and N_t in the two cases, respectively. Given the structure of $f_{opt} = \sum_{j=1}^{L} \beta_j v_j$, we have

$$Hf_{opt} = \left(\sum_{i=1}^{L} \alpha_i u_i v_i^H \right) \cdot \left(\sum_{j=1}^{L} \beta_j v_j \right) \tag{45}$$

$$= \sum_{i=1}^{L} \alpha_i \cdot \left(\sum_j \beta_j v_i^H v_j \right) u_i \tag{46}$$

and thus g_{opt} is a linear combination of $\{u_1, \ldots, u_L\}$. ∎

B. Proof of Theorem 2

Since $\text{SNR}_{rx} = \rho_f \cdot \frac{|g^H Hf|^2}{g^H g}$ is invariant to $\|g\|_2$, we let $g = \|g\|_2 \cdot \widetilde{g}$ where $\|\widetilde{g}\|_2 = 1$ (Constraint 1). The 2- and ∞-norm constraints on g are equivalent to $\|g\|_2 \leq 1$ and $\|g\|_\infty = \|g\|_2 \cdot \|\widetilde{g}\|_\infty \leq \frac{1}{\sqrt{N_r}}$ (Constraints 2 and 3). The received SNR maximization can then be recast as

$$\widetilde{g}_{opt} = \arg\max_{\widetilde{g}} \frac{\text{SNR}_{rx}}{\rho_f} = \arg\max_{\widetilde{g}} \frac{|\widetilde{g}^H Hf|^2}{\widetilde{g}^H \widetilde{g}} \tag{47}$$

subject to Constraints 1 to 3. Ignoring Constraints 2 and 3 in the above optimization, SNR_{rx} can be upper bounded as $\rho_f \cdot \|Hf\|_2^2$ with equality if $\widetilde{g} = \alpha \cdot Hf$ for some α. We now consider a specific choice $g = \frac{1}{\sqrt{N_r}} \cdot \frac{Hf}{\|Hf\|_\infty}$. We note that this choice is in $\mathcal{F}_\infty^{N_r}$ by satisfying all the three constraints since $\widetilde{g} = \frac{Hf}{\|Hf\|_2}$, $\|g\|_2 = \frac{\|Hf\|_2}{\sqrt{N_r} \cdot \|Hf\|_\infty} \leq 1$ and $\|g\|_2 \cdot \|\widetilde{g}\|_\infty = \frac{1}{\sqrt{N_r}}$. Further, the upper bound for SNR_{rx} is also met and this choice is optimal from $\mathcal{F}_\infty^{N_r}$.

Let f be the optimal beamformer from $\mathcal{F}_\infty^{N_t}$ that maximizes $f^H H^H Hf$ and let the magnitude of at least one of its entries not equal $\frac{1}{\sqrt{N_t}}$. Without loss in generality (by appropriate rotations with permutation matrices), let one of these entries be the first entry. Let f and $H^H H$ be partitioned as

$$f = \begin{bmatrix} \underbrace{f(1)}_{1 \times 1} \\ \underbrace{f_r}_{N_t - 1 \times 1} \end{bmatrix}, H^H H = \begin{bmatrix} \underbrace{h}_{1 \times 1} & \underbrace{h_r^H}_{1 \times N_t - 1} \\ \underbrace{h_r}_{N_t - 1 \times 1} & \underbrace{H_r}_{N_t - 1 \times N_t - 1} \end{bmatrix}. \tag{48}$$

With this partition, we have the following expansion:

$$f^H H^H Hf = |f(1)|^2 h + 2\text{Re}\left(f(1) \cdot f_r^H h_r\right) + f_r^H H_r f_r. \tag{49}$$

Since f is optimal, whatever be the choice of f_r, we should have $\angle f(1) = \angle h_r^H f_r$. Otherwise, we can find a better choice of $f(1)$ for the same f_r. With this optimal choice for $\angle f(1)$, (49) reduces to

$$f^H H^H Hf = |f(1)|^2 h + 2|f(1)| \cdot |f_r^H h_r| + f_r^H H_r f_r. \tag{50}$$

Clearly, (50) is increasing in $|f(1)|$ and thus $|f(1)| = \frac{1}{\sqrt{N_t}}$. Thus, the assumption that the magnitude of at least one of the entries of f is not $\frac{1}{\sqrt{N_t}}$ is untenable and we end up with a contradiction to the statement. This implies that equal gain transmit beamforming is optimal. ∎

C. Proof of Prop. 1

Let $f(i) = \frac{1}{\sqrt{N_t}} \cdot e^{j\theta_i}$ for some θ_i. With the matched filter structure for g and with H as in the statement of the proposition, $f^H H^H Hf$ is given as

$$\frac{\text{SNR}_{rx}}{\rho_f} = f^H H^H Hf = \sum_{i,k=1}^{N_t} h_i^H h_k \cdot e^{j(\theta_k - \theta_i)} \tag{51}$$

$$= \sum_{i=1}^{N_t} h_i^H h_i + 2 \sum_{k<i} \text{Re}\left(h_i^H h_k \cdot e^{j(\theta_k - \theta_i)}\right). \tag{52}$$

While the optimal beamforming vector requires a simultaneous optimization over $\{\theta_i\}$, we can rewrite the objective function as

$$f^H H^H Hf = \sum_{i=1}^{N_t} h_i^H h_i$$
$$+ 2 \sum_{i=1}^{N_t} \text{Re}\left(e^{-j\theta_i} \cdot \left(\sum_{k=1}^{i-1} e^{j\theta_k} \cdot h_i^H h_k \right) \right). \tag{53}$$

With a recursive structure as in (20), each term in (53) is maximized, even though the impact of this structure on the sum of these terms is unclear. ∎

D. Proof of Theorem 3

With $\{\Omega_j\}$ as sampling frequencies, we have

$$\min_{j=1,\ldots,J} |F(\Omega_j)|^2 \leq \frac{1}{J} \cdot \sum_{j=1}^{J} |F(\Omega_j)|^2 \tag{54}$$

$$= \frac{1}{J} \cdot f^H \left(\sum_{j=1}^{J} a(\Omega_j) a(\Omega_j)^H \right) f \tag{55}$$

$$\leq \frac{\lambda_{max}\left(\sum_{j=1}^{J} a(\Omega_j) a(\Omega_j)^H i \right)}{J} \tag{56}$$

where the last inequality follows from the Rayleigh coefficient of a Hermitian matrix and its largest eigenvalue. A straightforward argument shows that the $J = 2$ setting minimizes the above upper bound when $\Omega_0 = \frac{A \cdot 2\pi}{N_t}$ where $0 \leq A \leq 1$. Further, in this case, the choice $\Omega_2 = \frac{\pi}{2} + \frac{A \cdot \pi}{N_t}$ and $\Omega_1 = \frac{\pi}{2} - \frac{A \cdot \pi}{N_t}$ minimizes the upper bound resulting in

$$\lambda_{max}\left(\sum_{j=1}^{J} a(\Omega_j) a(\Omega_j)^H \right) = N_t + \left| \frac{\sin(N_t(\Omega_2 - \Omega_1)/2)}{\sin((\Omega_2 - \Omega_1)/2)} \right|. \tag{57}$$

Using this fact, the worst-case beamforming gain is seen to be

$$\text{BFGain} \leq$$

$$10 \log_{10}\left(\min\left(N_t, \frac{N_t}{2} + \frac{1}{2} \cdot \left| \frac{\sin\left(\frac{\overline{\Omega} \cdot N_t}{2 N_o. \text{ beams}} \right)}{\sin\left(\frac{\overline{\Omega}}{2 N_o. \text{ beams}} \right)} \right| \right) \right) \tag{58}$$

provided No. beams $\geq \frac{\overline{\Omega} \cdot N_t}{2\pi}$. In general, it is difficult to obtain closed-form expressions for the eigenvalues of $\sum_{j=1}^{J} \mathbf{a}(\Omega_j)\mathbf{a}(\Omega_j)^H$ with $J = 3, 4$ and this task is impossible if $J > 4$. Thus, in these settings (No. beams $< \frac{\overline{\Omega} \cdot N_t}{2\pi}$), the best-case (smallest) upper bound is obtained by minimizing the quantity in (56) over different choices of J and $\{\Omega_j\}$ leading to (38), where $\Omega_j \in \left[\Omega_c - \frac{\Omega_0}{2}, \Omega_c + \frac{\Omega_0}{2}\right]$ with $\Omega_0 = \frac{\overline{\Omega}}{\text{No. beams}} > \frac{2\pi}{N_t}$. ∎

REFERENCES

[1] F. Rusek et al., "Scaling up MIMO: Opportunities and challenges with very large arrays," IEEE Signal Process. Mag., vol. 30, no. 1, pp. 40–60, Jan. 2013.
[2] N. Bhushan et al., "Network densification: The dominant theme for wireless evolution into 5G," IEEE Commun. Mag., vol. 52, no. 2, pp. 82–89, Feb. 2014.
[3] F. Boccardi, R. W. Heath Jr., A. Lozano, T. L. Marzetta, and P. Popovski, "Five disruptive technology directions for 5G," IEEE Commun. Mag., vol. 52, no. 2, pp. 74–80, Feb. 2014.
[4] Qualcomm. (2013 Nov.) The 1000-X Data Challenge [Online]. Available: http://www.qualcomm.com/solutions/wireless-networks/technologies/1000x-data.
[5] F. Khan and Z. Pi, "An introduction to millimeter wave mobile broadband systems," IEEE Commun. Mag., vol. 49, no. 6, pp. 101–107, Jun. 2011.
[6] E. Torkildson, U. Madhow, and M. Rodwell, "Indoor millimeter wave MIMO: Feasibility and performance," IEEE Trans. Wireless Commun., vol. 10, no. 12, pp. 4150–4160, Dec. 2011.
[7] T. S. Rappaport et al., "Millimeter wave mobile communications for 5G cellular: It will work!" IEEE Access, vol. 1, pp. 335–349, May 2013.
[8] S. Rangan, T. S. Rappaport, and E. Erkip, "Millimeter wave cellular networks: Potentials and challenges," Proc. IEEE, vol. 102, no. 3, pp. 366–385, Mar. 2014.
[9] W. Roh et al., "Millimeter-wave beamforming as an enabling technology for 5G cellular communications: Theoretical feasibility and prototype results," IEEE Commun. Mag., vol. 52, no. 2, pp. 106–113, Feb. 2014.
[10] M. R. Akdeniz et al., "Millimeter wave channel modeling and cellular capacity evaluation," IEEE J. Sel. Areas Commun., vol. 32, no. 6, pp. 1164–1179, Jun. 2014.
[11] C. Lim, T. Yoo, B. Clerckx, B. Lee, and B. Shim, "Recent trend of multiuser MIMO in LTE-Advanced," IEEE Commun. Magaz., vol. 51, no. 3, pp. 127–135, Mar. 2013.
[12] V. Venkateswaran and A.-J. van der Veen, "Analog beamforming in MIMO communications with phase shift networks and online channel estimation," IEEE Trans. Signal Process., vol. 58, no. 8, pp. 4131–4143, Aug. 2010.
[13] J. Brady, N. Behdad, and A. M. Sayeed, "Beamspace MIMO for millimeter-wave communications: System architecture, modeling, analysis and measurements," IEEE Trans. Antennas Propag., vol. 61, no. 7, pp. 3814–3827, Jul. 2013.
[14] O. El Ayach, S. Rajagopal, S. Abu-Surra, Z. Pi, and R. W. Heath Jr., "Spatially sparse precoding in millimeter wave MIMO systems," IEEE Trans. Wireless Commun., vol. 13, no. 3, pp. 1499–1513, Mar. 2014.
[15] S. Hur, T. Kim, D. J. Love, J. V. Krogmeier, T. A. Thomas, and A. Ghosh, "Millimeter wave beamforming for wireless backhaul and access in small cell networks," IEEE Trans. Commun., vol. 61, no. 10, pp. 4391–4403, Oct. 2014.
[16] A. Alkhateeb, O. El Ayach, G. Leus, and R. W. Heath Jr., "Channel estimation and hybrid precoding for millimeter wave cellular systems," IEEE J. Sel. Topics Signal Process., vol. 8, no. 5, pp. 831–846, Oct. 2014.
[17] S. Sun, T. S. Rappaport, R. W. Heath Jr., A. Nix, and S. Rangan, "MIMO for millimeter wave wireless communications: Beamforming, spatial multiplexing, or both?" IEEE Commun. Mag., vol. 52, no. 12, pp. 110–121, Dec. 2014.
[18] H. Zhao et al., "28 GHz millimeter wave cellular communication measurements for reflection and penetration loss in and around buildings in New York City," in Proc. IEEE Int. Conf. Commun., Jun. 2013, pp. 5163–5167.
[19] A. M. Sayeed, "Deconstructing multi-antenna fading channels," IEEE Trans. Signal Process., vol. 50, no. 10, pp. 2563–2579, Oct. 2002.
[20] A. M. Sayeed and V. Raghavan, "Maximizing MIMO capacity in sparse multipath with reconfigurable antenna arrays," IEEE J. Sel. Topics Signal Process., vol. 1, no. 1, pp. 156–166, Jun. 2007.
[21] V. Raghavan and A. M. Sayeed, "Sublinear capacity scaling laws for sparse MIMO channels," IEEE Trans. Inf. Theory, vol. 57, no. 1, pp. 345–364, Jan. 2011.
[22] T. K. Y. Lo, "Maximum ratio transmission," IEEE Trans. Commun., vol. 47, no. 10, pp. 1458–1461, Oct. 1999.
[23] O. El Ayach, R. W. Heath Jr., S. Abu-Surra, S. Rajagopal, and Z. Pi, "The capacity optimality of beam steering in large millimeter wave MIMO systems," in Proc. IEEE Conf. Signal Process. Adv. Wireless Commun., Cesme, Turkey, Jun. 2012, vol. 1, pp. 100–104.
[24] D. J. Love and R. W. Heath Jr., "Equal gain transmission in multiple-input multiple-output wireless systems," IEEE Trans. Commun., vol. 51, no. 7, pp. 1102–1110, Jul. 2003.
[25] Z. Pi, "Optimal MIMO transmission with per-antenna power constraints," in Proc. IEEE Global Telecommun. Conf., Anaheim, CA, USA, Dec. 2012, vol. 1, pp. 2493–2498.
[26] T. Dahl, N. Christophersen, and D. Gesbert, "Blind MIMO eigenmode transmission based on the algebraic power method," IEEE Trans. Signal Process., vol. 52, no. 9, pp. 2424–2431, Sep. 2004.
[27] A. L. Swindlehurst, E. Ayanoglu, P. Heydari, and F. Capolino, "Millimeter-wave massive MIMO: The next wireless revolution?" IEEE Commun. Mag., vol. 52, no. 9, pp. 56–62, Sep. 2014.
[28] R. O. Schmidt, "Multiple emitter location and signal parameter estimation," IEEE Trans. Antennas Propag., vol. AP-34, no. 3, pp. 276–280, Mar. 1986.
[29] R. Roy and T. Kailath, "ESPRIT: Estimation of signal parameters via rotational invariance techniques," IEEE Trans. Acoust. Speech Signal Process., vol. 37, no. 7, pp. 984–995, Jul. 1989.
[30] H. Krim and M. Viberg, "Two decades of array signal processing research: The parametric approach," IEEE Signal Process. Mag., vol. 13, no. 4, pp. 67–94, Jul. 1996.
[31] D. J. Love, R. W. Heath Jr., V. K. N. Lau, D. Gesbert, B. D. Rao, and M. Andrews, "An overview of limited feedback in wireless communication systems," IEEE J. Sel. Areas Commun., vol. 26, no. 8, pp. 1341–1365, Oct. 2008.
[32] D. J. Love, R. W. Heath Jr., and T. Strohmer, "Grassmannian beamforming for multiple-input multiple-output wireless systems," IEEE Trans. Inf. Theory, vol. 49, no. 10, pp. 2735–2747, Oct. 2003.
[33] K. K. Mukkavilli, A. Sabharwal, E. Erkip, and B. Aazhang, "On beamforming with finite rate feedback in multiple antenna systems," IEEE Trans. Inf. Theory, vol. 49, no. 10, pp. 2562–2579, Oct. 2003.
[34] S. Rajagopal, "Beam broadening for phased antenna arrays using multibeam subarrays," in Proc. IEEE Int. Conf. Commun., Ottawa, ON, Canada, Jun. 2012, vol. 1, pp. 3637–3642.
[35] C. Jeong, J. Park, and H. Yu, "Random access in millimeter-wave beamforming cellular networks: Issues and approaches," IEEE Commun. Mag., vol. 53, no. 1, pp. 180–185, Jan. 2015.
[36] H. S.-Ghadikolaei, C., Fischione, G., Fodor, P. Popovski, and M. Zorzi, "Millimeter wave cellular networks: A MAC layer perspective," IEEE Trans. Commun., vol. 63, no. 10, pp. 3437–3458, Oct. 2015.
[37] C. N. Barati et al., "Directional cell discovery in millimeter wave cellular networks," IEEE Trans. Wireless Commun., vol. 14, no. 12, pp. 6664–6678, Dec. 2015.
[38] A. A. M. Saleh and R. Valenzuela, "A statistical model for indoor multipath propagation," IEEE J. Sel. Areas Commun., vol. 5, no. 2, pp. 128–137, Feb. 1987.
[39] A. M. Sayeed, V. Raghavan, and J. H. Kotecha, "Capacity of space-time wireless channels: A physical perspective," in Proc. IEEE Inf. Theory Workshop, San Antonio, TX, USA, Oct. 2004, pp. 434–439.
[40] D. Gesbert, H. Bölcskei, D. A. Gore, and A. J. Paulraj, "Outdoor MIMO wireless channels: Models and performance prediction," IEEE Trans. Commun., vol. 50, no. 12, pp. 1926–1934, Dec. 2002.
[41] A. J. Goldsmith, S. A. Jafar, N. Jindal, and S. Vishwanath, "Capacity limits of MIMO channels," IEEE J. Sel. Areas Commun., vol. 21, no. 5, pp. 684–702, Jun. 2003.

[42] V. Raghavan, A. S. Y. Poon, and V. V. Veeravalli, "MIMO systems with arbitrary antenna array architectures: Channel modeling, capacity and low-complexity signaling," in *Proc. IEEE Asilomar Conf. Signals Syst. Comput.*, Pacific Grove, CA, USA, Nov. 2007, vol. 1, pp. 1219–1223.

[43] V. Raghavan, S. V. Hanly, and V. V. Veeravalli, "Statistical beamforming on the Grassmann manifold for the two-user broadcast channel," *IEEE Trans. Inf. Theory*, vol. 59, no. 10, pp. 6464–6489, Oct. 2013.

[44] V. Raghavan, S. Subramanian, J. Cezanne, and A. Sampath, "Directional beamforming for millimeter-wave MIMO systems," in *Proc. IEEE Global Telecommun. Conf.*, San Diego, CA, USA, Dec. 2015, Extended version, [Online]. Available: http://www.arxiv.org/abs/1601.02380.

[45] G. H. Golub and C. F. Van Loan, *Matrix Computations*, 3rd ed. Baltimore, MD, USA: The Johns Hopkins Univ. Press, 1996.

[46] V. Raghavan, A. M. Sayeed, and N. Boston, "When is limited feedback for transmit beamforming beneficial?" in *Proc. IEEE Int. Symp. Inf. Theory*, Adelaide, Australia, Sep. 2005, vol. 1, pp. 1544–1548.

[47] V. Raghavan, R. W. Heath Jr., and A. M. Sayeed, "Systematic codebook designs for quantized beamforming in correlated MIMO channels," *IEEE J. Sel. Areas Commun.*, vol. 25, no. 7, pp. 1298–1310, Sep. 2007.

[48] M. Wax and T. Kailath, "Detection of signals by information theoretic criteria," *IEEE Trans. Acoust. Speech Signal Process.*, vol. ASSP-33, no. 4, pp. 387–392, Apr. 1985.

[49] J. A. Fessler and A. O. Hero, "Space-alternating generalized expectation maximization algorithm," *IEEE Trans. Signal Process.*, vol. 42, no. 10, pp. 2664–2677, Oct. 1994.

[50] B. H. Fleury, M. Tschudin, R. Heddergott, D. Dahlhaus, and K. I. Pedersen, "Channel parameter estimation in mobile radio environments using the SAGE algorithm," *IEEE J. Sel. Areas Commun.*, vol. 17, no. 3, pp. 434–450, Mar. 1999.

[51] A. Richter, M. Landmann, and R. Thoma, "RIMAX—A flexible algorithm for channel parameter estimation from channel sounding measurements," *Proc. 9th Manage. Committee Meeting (COST273)*, Athens, Greece, Jan. 2004, COST 273 TD(04)045.

[52] D. Ramasamy, S. Venkateswaran, and U. Madhow, "Compressive tracking with 1000-element arrays: A framework for multi-Gbps mm-wave cellular downlinks," in *Proc. Annu. Allerton Conf. Commun. Control Comput.*, Allerton, IL, USA, Oct. 2012, pp. 690–697.

[53] P. Schniter and A. M. Sayeed, "Channel estimation and precoder design for millimeter-wave communications: The sparse way," in *Proc. IEEE Asilomar Conf. Signals Syst. Comput.*, Nov. 2014, pp. 273–277.

[54] B. Recht, M. Fazel, and P. A. Parrilo, "Guaranteed minimum-rank solutions of linear matrix equations via nuclear norm minimization," *SIAM Rev.*, vol. 52, no. 3, pp. 471–501, Aug. 2010.

[55] A. Adhikary *et al.*, "Joint spatial division and multiplexing for mm-Wave channels," *IEEE J. Sel. Areas Commun.*, vol. 32, no. 6, pp. 1239–1255, Jun. 2014.

[56] C. A. Balanis, *Antenna Theory: Analysis and Design*, 3rd ed. New York, NY, USA: Wiley-Interscience, 2005.

Juergen Cezanne received the Dipl.-Ing. and Dr.-Ing. degrees in electrical engineering from Technical University Darmstadt, Darmstadt, Germany, in 1986 and 1991, respectively. Currently he is a Principal Engineer with Qualcomm Corporate R&D, Bridgewater, NJ, USA. He has been with Qualcomm, Inc., since 2006, and prior to that with Flarion Technologies between 2003 and 2005. From 1991 to 2003, he was with Bell Labs at their Murray Hills and Holmdel locations. His research interests include millimeter wave wireless research topics including system design, standardization, prototyping, and firmware issues.

Sundar Subramanian received the M.S. and Ph.D. degrees in electrical and computer engineering from the University of Texas at Austin, Austin, TX, USA, in 2004 and 2008, respectively. He was with Qualcomm, Inc., for the past 8 years and has worked on many areas including PHY/MAC design for D2D systems and vehicular communications. His research interests include scheduling and networking techniques for heterogeneous networks and PHY/MAC algorithms for cellular and mobile communications, system design and modeling for next generation millimeter wave networks. He is named a co-inventor on 30 granted patents on wireless networks.

Ashwin Sampath received the Ph.D. degree in electrical engineering from Rutgers University, New Brunswick, NJ, USA. He is currently the Senior Director of Technology at Corporate R&D, Qualcomm, Inc., NJ, USA. He has been with Qualcomm, Corporate R&D, since 2005, where he has led projects related to dense small-cell networks, topics in LTE-Advanced, 3G/4G multi-mode wireless modem design for small-cell ASICs and femto-cell SoC architecture. Prior to joining Qualcomm, he was with Texas Instruments from 2003 to 2005, leading HSDPA systems engineering for a mobile SoC and before that, was Distinguished Member of Technical Staff at Bell Labs from 1997 to 2003. He has over 90 issued patents. His research interests include wide-ranging topics that straddle millimeter wave research such as channel measurements/modeling, system design, standardization and prototyping.

Vasanthan Raghavan (S'01–M'06–SM'11) received the B.Tech degree in electrical engineering from the Indian Institute of Technology at Madras, Chennai, India, in 2001, and the M.S. and Ph.D. degrees in electrical and computer engineering, in 2004 and 2006, respectively, and the M.A. degree in mathematics, in 2005, all from the University of Wisconsin, Madison, WI, USA. He is currently with the New Jersey Research Center of Qualcomm, Inc. His research interests include multiantenna communication techniques, information theory, quickest changepoint detection, and random matrix theory.

Ozge Koymen received the B.S. degree in electrical and computer engineering from Carnegie Mellon University, Pittsburgh, PA, USA, in 1996, and the M.S. and Ph.D. degrees in electrical engineering from Stanford University, Stanford, CA, USA, in 1997 and 2003, respectively. He has been with Qualcomm, Inc., in the Corporate R&D Division, since 2006, where he is currently a Principal Engineer working on 5G millimeter-wave access systems. He was earlier a member of Flarion Technologies developing OFDMA systems between 2003 and 2006. His prior experience includes consulting work for TRW (1996–2000) and Impinj, Inc., (2000–03).